Enhancing Energy Storage Capabilities of Cobalt Sulfide by Controlling Synthesis Growth Parameters

M.Sc. Thesis

by

SHIVANSH RAJ PANDEY

DEPARTMENT OF PHYSICS

INDIAN INSTITUTE OF TECHNOLOGY INDORE

May 2024

Enhancing Energy Storage Capabilities of Cobalt Sulfide by Controlling Synthesis Growth Parameters

A THESIS

Submitted in partial fulfillment of the
requirements for the award of the degree
of
Master of Science

by

SHIVANSH RAJ PANDEY

DEPARTMENT OF PHYSICS
INDIAN INSTITUTE OF TECHNOLOGY INDORE

May 2024

INDIAN INSTITUTE OF TECHNOLOGY INDORE

CANDIDATE'S DECLARATION

I hereby certify that the work being presented in the thesis entitled **Enhancing Energy Storage Capabilities of Cobalt Sulfide by Controlling Synthesis Growth Parameters** in the partial fulfillment of the requirements for the award of the degree of **MASTER OF SCIENCE** and submitted in the **DEPARTMENT OF PHYSICS, Indian Institute of Technology Indore**, is an authentic record of my own work carried out during the time period from May 2023 to May 2024 under the supervision of Prof. Rajesh Kumar, Professor, Department of Physics, IIT Indore

The matter presented in this thesis has not been submitted by me for the award of any other degree of this or any other institute.

14/05/2024

Signature of the student with date
(SHIVANSH RAJ PANDEY)

This is to certify that the above statement made by the candidate is correct to the best of my knowledge.

14/05/2024

Signature of the Supervisor of
M.Sc. thesis (with date)
(Prof. Rajesh Kumar)

SHIVANSH RAJ PANDEY has successfully given his M.Sc. Oral Examination held on **16th May 2024**.

Signature of Supervisor of MSc thesis
Date: 22/05/2024

Convener, DPGC
Date: 22/05/2024

ACKNOWLEDGEMENTS

I wholeheartedly acknowledge that the completion of my thesis work was a collective effort involving the support and guidance of numerous individuals, without whom this endeavor would not have been possible. It is with immense gratitude that I express my appreciation to each one of them. First and foremost, I extend my deepest gratitude to my thesis supervisor Prof. Rajesh Kumar, Department of Physics at the Indian Institute of Technology Indore, for his constant support, invaluable patience, and critical feedback. I couldn't have completed this journey without his generous knowledge and ideas and most importantly his selfless guidance. My progress toward finishing my M.Sc. project thesis was fueled by Prof. Rajesh's vast knowledge and methodical approach, which served as a continual source of inspiration. I am truly grateful to my committed lab members for their consistent support of my work. I am sincerely thankful to my senior Mr. Love Bansal for his great help with data analysis, graphing, sample preparation, and characterization. Additionally, I admire Mr. Deb Kumar Rath, Ms. Bhumika Sahu, Ms. Nikita Ahlawat, and my batchmate Mr. MD Sahid Ahmed for their encouragement and assistance during this project. I also acknowledge Dr. Nitin Upadhyay for his technical assistance in XRD measurements at SIC (IIT Indore). Furthermore, I extend my gratitude to the entire faculty and staff of the Department of Physics, IIT Indore, for their constant support and assistance.

Without the support of friends, no journey is complete, and mine too had many of them. I thank my friends Deepak Sain, Nishi Thakur, Harshit Joshi, Nilesh Tungaria, and Vishal for their

unwavering encouragement and support. Throughout this journey, your friendship has been a source of inspiration and strength.

Finally, and from the bottom of my heart, I would like to thank my father, Mr. Rajendra Kumar Pandey, whose knowledge, wisdom, and support made this journey possible, and my mother, Mrs. Shashi Pandey, for all the non-repayable hard work she has done to make me who I am today.

Shivansh Raj Pandey

Dedicated to my family and teachers

Abstract

This thesis investigates the electrochemical performance of cobalt sulfide Co_xS_y films deposited via pulse and continuous electrodeposition methods for energy storage applications. Supercapacitors, known for their high-power density and rapid charge-discharge capabilities, represent a critical technology in the field of energy storage. However, enhancing their energy density remains a significant challenge, often addressed through the exploration of advanced electrode materials such as transition metal sulfides. The pulse and continuous electrodeposition methods are utilized to fabricate cobalt sulfide films, with the pulse method offering precise control over deposition parameters. Scanning electron microscopy (SEM) and X-ray diffraction (XRD) analyses reveal distinct morphologies and surfaces for the deposited films. Electrochemical characterization, including cyclic voltammetry (CV) and galvanostatic charge-discharge (GCD) measurements, demonstrates superior specific capacitance for the pulse-electrodeposited Cobalt sulfide films compared to their continuous counterparts. This enhanced performance is attributed to the uniform morphology achieved through the pulse deposition technique, facilitating improved charge storage and diffusion kinetics. In conclusion, this research contributes to the advancement of electrode materials for supercapacitors by elucidating the influence of electrodeposition techniques on the energy storage properties of cobalt sulfide.

TABLE OF CONTENTS

LIST OF FIGURES

Figure 3.29 (a) Potential dependent CV curve at a scan rate of 50 mV/s (b) Specific capacitance vs Potential window curve for PED cobalt sulfide//activated carbon device [46]

LIST OF TABLES

ACRONYMS

XRD X-ray Diffraction

SEM Scanning Electron Microscopy

EDX Energy Dispersive X-ray Spectroscopy

SC Supercapacitor

EDLC Electrochemical double-layer capacitor

NMP N-methyl-2-pyrrolidone

PED Pulse Electrodeposited

CED Continuous Electrodeposited

IUPAC International Union of Pure and Applied Chemistry

CV Cyclic Voltammetry

GCD Galvanostatic Charge Discharge

EIS Electrochemical Impedance Spectroscopy

IPA Isopropyl Alcohol

FTO Fluorine-doped Tin oxide

WE Working Electrode

RE Reference Electrode

CE Counter Electrode

Chapter 1

INTRODUCTION

1.1 General Background

The growth of renewable energy sources, such as solar, wind, ocean, and biomass, has been spurred by the gradual depletion of fossil fuels (petroleum, coal, natural gas, etc.) and the rise in CO_2 emissions[1–3]. High energy/power and long-lasting energy storage systems are typically needed to use such energy sources efficiently[4,5]. High-performance power sources are becoming more and more in demand as electric cars, smart grids, and other portable and wearable gadgets become more widely used[6,7]. Based on the survey on total world energy consumption conducted by the Energy Information Administration (EIA), fossil fuels make up the bulk of the world's current primary energy sources[8]. Sustainable and renewable energy sources have attracted great interest nowadays due to the decrease of natural reserves. As a result, there has been a lot of research done on the potential for gathering energy from the sun, wind, water, etc. The time periodicity of energy generation from these sources, for instance, the shift in daylight from day to night and the intermittent nature of the wind, is a major disadvantage[8]. Energy storage has drawn a lot of interest since it is a crucial transitional phase between these energy resources and flexible energy applications[9–11]. It is obvious that batteries and supercapacitors, two types of electrochemical energy storage devices, will be essential in these domains[12–15]. Advanced batteries, like lithium-ion batteries, are expected to power large-scale electric vehicles in the near future due to their capacity to store large amounts of energy via bulk redox reactions in

electrodes[16,17]. These batteries are already widely used in portable electronics like laptop computers[18]. Supercapacitors, in contrast to batteries, often have a high power density; they can store energy for brief periods of time and then release it when needed[19].

1.2 Supercapacitors (SCs)

The word "supercapacitors" refers to a broad category of electrochemical capacitors[20]. They are a high-capacity device that sits between electrolytic capacitors and rechargeable batteries[21]. Their capacitance values are significantly higher than those of traditional capacitors, but they have lower voltage limits. Compared to traditional capacitors, they usually store 10–100 times more energy per unit volume or mass. Compared to batteries, supercapacitors have a far faster rate of acceptance and delivery of charge as well as a much higher tolerance for charge and discharge cycles[22,23]. SCs can be divided into electric double layer capacitors (EDLCs), pseudo-/Faradaic capacitors (PCs), and hybrid capacitors (HCs) according to the mode of energy storage[5,18,24]. Supercapacitors are also divided into two groups based on the charge storage mechanism: pseudocapacitors (Faradaic) and electric double-layer supercapacitors (non-Faradaic, or EDLC) (Figure 1.1). Furthermore, depending on the material of the electrode, supercapacitor devices are divided into symmetric and asymmetric categories[25–27]. In an asymmetric supercapacitor, one electrode is of the supercapacitor type while the other is of the battery type. In a symmetric supercapacitor, both electrodes are of the same kind[28]. As an electrode material for EDLC-type

supercapacitors, carbon-based materials[29] like graphene[30], carbon nanotubes[31], activated carbon[31], carbon nanofibers[32], and mesoporous carbon[33] are commonly utilized because of their high specific surface area, high cyclic stability, high chemical stability, high electrical conductivity, and environmental friendliness. Pseudocapacitors are useful in boosting energy density[5,34]. Typically, conducting polymers, transition metal oxides (TMOs), and hydroxides make pseudocapacitors[14,35,36]. Pseudocapacitance arises from the electrical charge transport in the redox process[37,38].

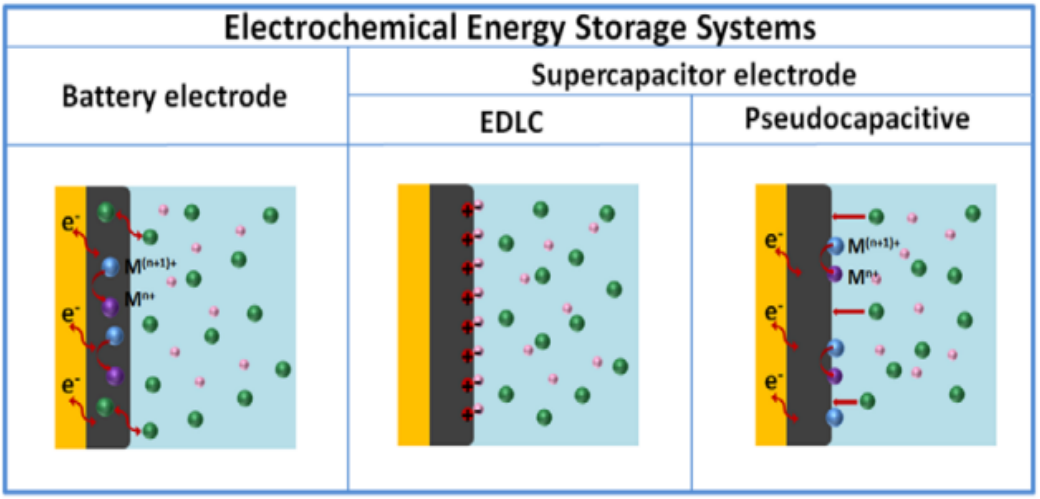

Figure 1.1 Schematic diagram comparing the fundamental charge storage mechanisms of electrode materials in batteries and supercapacitors[18].

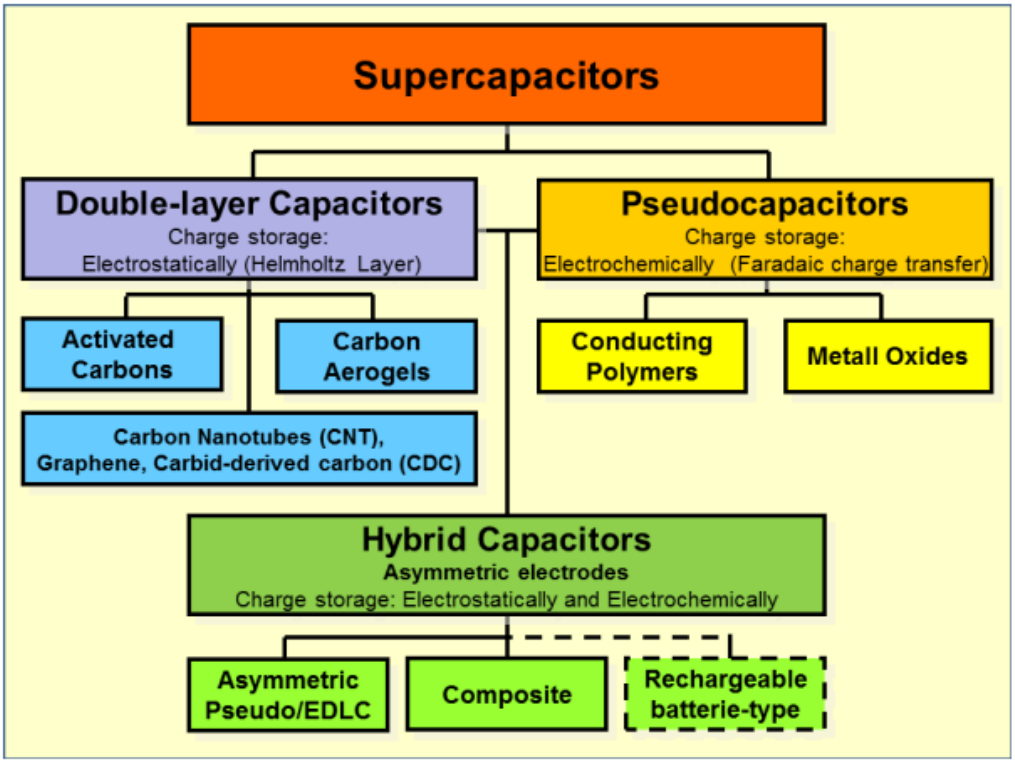

Figure 1.2 Supercapacitor types; electrochemical double-layer capacitors and pseudocapacitors as well as hybrid capacitors are defined over their electrode designs[5]

1.3 Performance parameters

Specific capacitance

Specific capacitance can be calculated using cyclic voltammetry (CV), galvanostatic charge-discharge (GCD), and electrochemical impedance spectroscopy (EIS).

From the CV plot, scan rate-dependent specific capacitance is given by[39],

$$C_s = \frac{\oint IdV}{2\nu m \Delta V}, \quad (1)$$

Where $\oint IdV$ is the area under the CV curve, m is the mass of the active material, ΔV is the potential window of the CV curve.

From the GCD plot, current density-dependent specific capacitance is given by[40],

$$C_s = \frac{I\,\Delta t_d}{m\,\Delta V}, \quad (2)$$

Where C_s is the specific capacitance, Δt_d is discharging time, m is the deposited mass, I is the current and ΔV is the discharging potential window.

From the EIS plot frequency-dependent specific capacitance is given by[41],

$$C_s = \frac{-1}{2\pi f Z''}, \quad (3)$$

Where Z" is the imaginary component of impedance.

Energy and Power Densities

Energy density is the amount of energy stored per unit mass (Wh Kg^{-1}) or per unit volume (Wh cm^{-3}). Energy density is a function of the specific capacitance and operating voltage of the device as shown in below equation[42] :

$$E = \frac{1}{2} C V^2, \quad (4)$$

Where E is the specific energy density (Wh Kg^{-1}), C is the specific capacitance (F g^{-1}), and V is the operating voltage (Volt).

Power density measures the ability to deliver power. In other words, it is how quickly the energy storage system can discharge the stored energy per unit mass or volume. Power density is calculated using the following equation[42]:

$$P = \frac{E}{\Delta t}, \qquad (5)$$

Where P is the power density (W Kg^{-1}), E is the energy density (Wh Kg^{-1}), and **Δ**t is the time (h).

Cyclic stability Test

Another crucial supercapacitor property, charge-discharge cycle stability, is tested to ensure that it performs well enough to be used in future energy storage systems.

1.4 Why Cobalt sulfide?

Because of their unique physical and chemical characteristics, metal chalcogenides have emerged as a material of interest for electronic, optical, and electrochemical applications in recent years[43–45]. Applications of metal chalcogenides, including cobalt, nickel, vanadium, and molybdenum sulfides, have been researched for electrochemical supercapacitors[43,46–48]. Additional evidence about the notable modifications to these materials' specific capacitance through different size, shape, hierarchical structures, and frequently nanohybrids with other materials can be found in the literature[44,49]. Cobalt sulfides are the most desirable of the metal chalcogenides because of their special optical, magnetic, electrical, and catalytic qualities[50]. There are several different phases of cobalt sulfide, including amorphous CoS_x, CoS, CoS_2, Co_3S_4, etc[47].

1.5 Motivation of This Study

This study aims to:

(a) Investigate the morphological, structural, and electrochemical properties of cobalt sulfide films synthesized via continuous electrodeposition and pulse electrodeposition method

(b) Compare the specific capacitance, charging-discharging time, etc. of the electrodes prepared by these two methods.

(c) Elucidate the relationship between the electrodeposition parameters, film morphology, and supercapacitor performance to guide future design and optimization of electrode materials.

Electrodeposition is a versatile and straightforward method to fabricate supercapacitor electrodes with controlled nanostructures that can potentially enhance the electrochemical performance[51]. However, the impact of different electrodeposition techniques on the morphology, structure, and electrochemical properties of cobalt sulfide films is not thoroughly explored. Among various electrodeposition strategies, continuous and pulse electrodeposition methods provide distinct pathways for material synthesis, affecting the adherence, uniformity, crystallinity, and electrochemical activity of the deposited films[52].

Chapter 2

EXPERIMENTAL TECHNIQUES

2.1 Material Synthesis

2.1.1 Material Used

For this work, several kinds of chemical compounds were purchased from Alfa Aesar/Sigma-Aldric commercially and used as supplied. Cobalt Nitrate Hexahydrate and Thiourea were used for the synthesis of cobalt sulfide films. For device fabrication, activated carbon (AC) and N-methyl-2-pyrrolidone (NMP) were used. Potassium hydroxide (KOH) pellets were used to make KOH electrolytes.

2.1.2 Synthesis Method

Films of Cobalt sulfide were prepared on fluorine-doped tin oxide (FTO) glass substrates using the electrodeposition method. Before the deposition, FTO glass substrates were cleaned using isopropyl alcohol (IPA) and acetone in an ultrasonic bath. Firstly, 87 mg Cobalt Nitrate Hexahydrate ($Co(NO_3)_2.6H_2O$) and 170 mg Thiourea ($SC(NH_2)_2$), taken as Cobalt and Sulphur precursors, respectively, were added in 20 mL of deionized water[53]. Then the solution was kept for stirring on a magnetic stirrer for 30 minutes at 50^o C temperature (Figure 2.1 (a)). This solution was further taken for the deposition of Cobalt sulfide films. After the film deposition, these FTO electrodes were put inside the vacuum oven for 120 minutes at 60^o C. The deposited films were utilized for additional characterization and subsequently for device construction and application

(a)

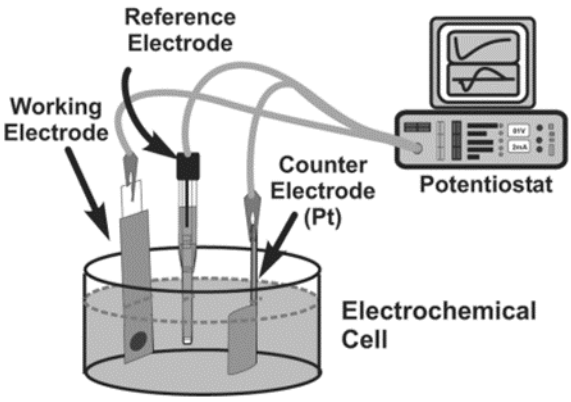

(b)

Figure 2.1. (a) Electrolyte solution (used for electrodeposition) on a magnetic stirrer **(b)** Three-electrode cell setup connected to a potentiostat[54]

Electrodeposition Method

The electrochemical process of electrodeposition facilitates the creation of solid deposits on the surface of conductive substances. It is a highly relevant process from a commercial standpoint, serving as the foundation for numerous industrial uses such metal plating, electro-winning, and refining. This method's primary benefit is its total control over thickness and homogeneity. Furthermore, it is discovered that the films formed using this technique are incredibly durable and robust, forming a very strong bond with the substrate.

The machine used for the electrodeposition process was Metrohm-Multi Autolab M204potenstiostat. The setup consists of a three-electrode cell system, filled with a solution called an electrolyte (Figure 2.1(b)). These three electrodes are:

1. ***Working Electrode (WE):*** The substrate (FTO in this case) is usually treated as a working electrode onto which material is to be deposited.
2. ***Reference Electrode (RE):*** It is an electrode that has a stable and well-known electrode potential. Silver chloride electrode (Ag/AgCl in 3M KCl) is the most common reference electrode. It offers a consistent reference potential for the electrochemical measurements. Other common reference electrodes are SHE (Standard Hydrogen Electrode), Standard Calomel Electrode, etc.
3. ***Counter Electrode (CE):*** It is also known as an auxiliary electrode. Its basic job is to allow the current passage through WE thus separating its path from RE. It is typically composed of inert materials such as Pt, Au, or glassy carbon. This electrode commonly remains uninvolved in the electrochemical reaction.

The fundamental process comprises a redox reaction occurring in the electrolytic solution as a result of an externally supplied bias or current. The film finally deposits on the top of the substrate as a result of electrons moving within the electrolyte and through its outer layer. The film deposition process is carried out using these two techniques-

- **Continuous Electrodeposition (CED):** In this adaptation, a constant potential (-0.9V in this case) is applied to the electrode for a prolonged period. This process involves maintaining the fixed potential where the material of interest is continuously reduced (or oxidized) onto the substrate.
- **Pulse Electrodeposition (PED):** Pulse electrodeposition involves applying a potential to the electrode in a series of on/off cycles (pulses). During the "on" phase, the potential is set to a level (-0.9V in this case) that facilitates deposition.

During the "off" phase, no potential is applied, allowing relaxation of the system, diffusion of the reactants back to the electrode surface, or stabilization of the deposited layer.

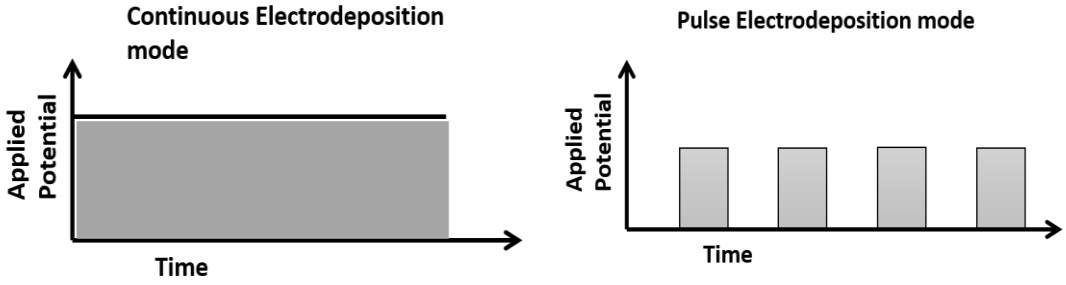

Figure 2.2 Input waveform of continuous electrodeposition and pulse electrodeposition mode

2.1.3 Device Fabrication

2.24g of Potassium hydroxide pellets were dissolved into 20 mL DI water to make a 2M aqueous KOH electrolyte solution. For the fabrication of the supercapacitor device, Cobalt sulfide deposited FTO and activated carbon deposited FTO were chosen as positive and negative electrodes, respectively and Whatman filter paper, saturated in 2M KOH electrolyte for some time, was chosen as a separator. The deposition of Cobalt sulfide film onto the FTO substrate via the electrodeposition method has already been discussed in section 2.1.2. To make activated carbon material electrodes, we have chosen the drop-casting method.

Drop casting method

This is a simple yet effective technique used for depositing thin films onto substrates. It is widely employed in research laboratories and small-scale production settings due to its ease of use, low caste, and versatility.

In our work, 100 mg of Activated carbon (AC) and 10 mL of N-methyl-2-pyrrolidone (NMP) were taken in mortar and pestle and this mixture was ground for 10-15 minutes. Then 50 µL of this solution was drop cast onto 1x1 cm^2 area of a clean FTO substrate and was kept inside an oven at 120^o C for overnight drying. The use of NMP-based slurries helps in achieving strong adhesion between the activated carbon particles and the current collector. The separator was placed between the two electrodes and then sealed entirely with epoxy parafilm to ensure that there was no interchange of oxygen ions from the atmosphere to the device, as shown in Figure 2.3.

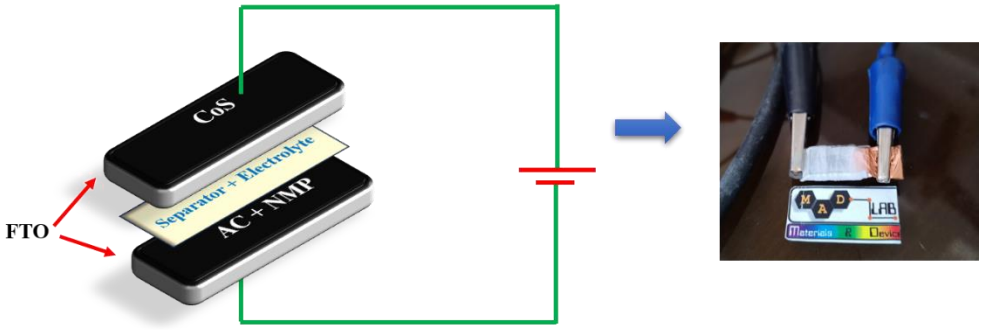

Figure 2.3 Schematic depiction of supercapacitor device fabrication

2.2 Characterization Techniques

2.2.1 X-ray Diffraction (XRD)

X-ray Diffraction (XRD) is a powerful non-destructive technique used to characterize the crystalline nature of materials. By measuring the diffraction patterns of X-rays that are incident upon and scattered by a material, XRD provides detailed information about the crystallographic structure, chemical composition, and physical properties of the sample. XRD operates on the principle of elastic scattering of X-rays from the electron clouds of atoms within a material. When X-rays interact with a crystal lattice, they may be diffracted according to **Bragg's Law**, $n\lambda=2d\sin\theta$ (Figure 2.4), where λ is the wavelength of the X-rays, d is the

distance between lattice planes, θ is the angle of incidence, and n is an integer. This diffraction occurs at specific angles for each material based on its unique crystal structure.

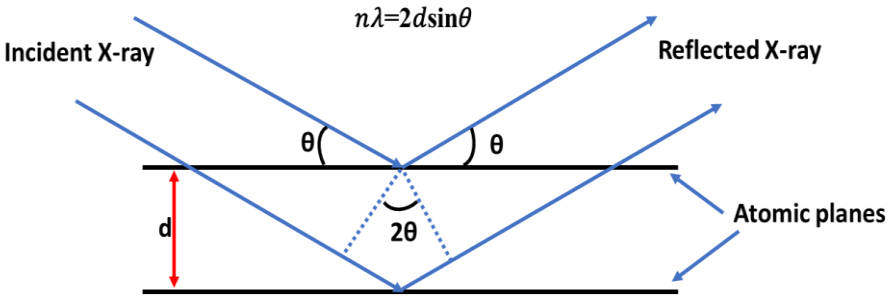

Figure 2.4 Schematic illustration of Bragg's law.

X-ray diffraction (XRD) measurements were conducted using a Bruker D2-Phaser diffractometer at a Cu Kα wavelength of 1.5406 Å.. The Schematic of an X-ray diffractometer is shown in Figure 2.5. The diffraction patterns obtained were analyzed using PowDLL Converter and Origin software to identify the crystalline phases present in the samples. Peak positions and intensities were compared against standard database entries from JCPDS (Joint Committee on Powder Diffraction Standards) to confirm the identity of phases.

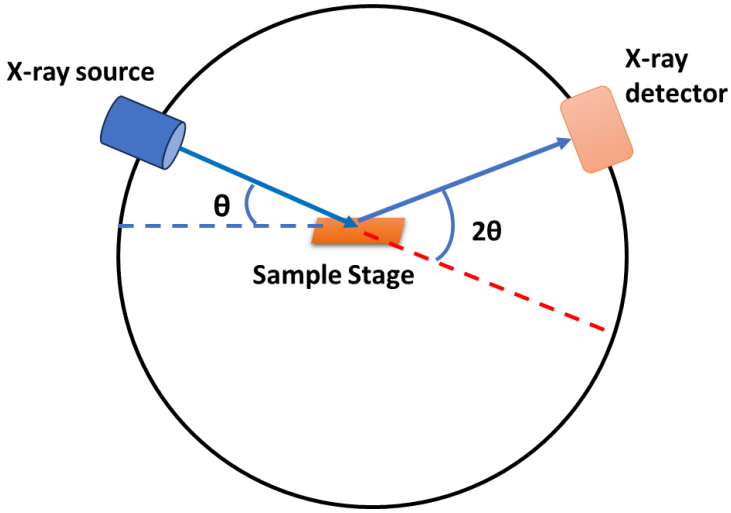

Figure 2.5 Schematic of X-ray diffractometer.

2.2.2 Raman Spectroscopy

Raman spectroscopy is an experimental spectroscopic technique that identifies a molecule's vibrational modes and, in turn, provides details on the structural fingerprint. The Raman spectra was recorded using a Horiba Jobin-Yvon Raman spectrometer and a 633 nm excitation laser (with the lowest power possible to prevent laser-induced heating).

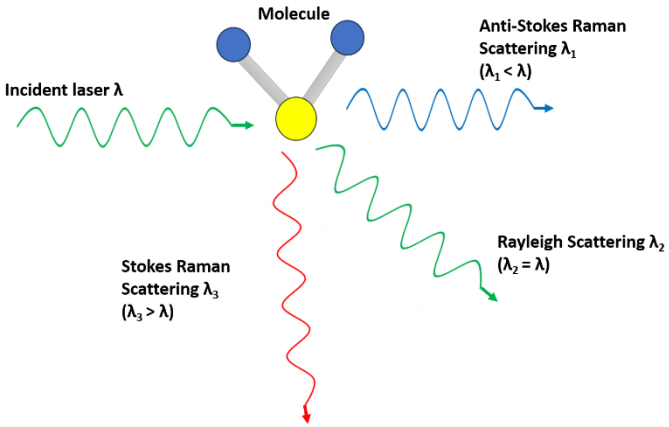

Figure 2.6 Schematic showing the basic mechanism of Raman spectroscopy.

The sample is first stimulated by a suitable wavelength of light, which causes the molecule to scatter off and remain in a higher excited state. When the molecule vibration returns to its ground state, it generates three different types of photons: two with higher (anti-stokes) or lower (stokes) energy than the initial photon, and one with the same energy as the first photon (Rayleigh scattering) (Figure 2.6). The Stokes line has a higher intensity than the anti-Stokes line. Raman spectroscopy is a non-corrosive spectroscopic method, wavenumbers are commonly used to express the corresponding Raman shifts.

2.2.3 Scanning Electron Microscopy (SEM)

Scanning Electron Microscopy (SEM) is a powerful imaging technique used to examine the surface structure and morphology of materials at high magnification. By using a focused beam of electrons, SEM allows for the detailed visualization of sample surfaces, providing critical insights into the material's topographical, compositional, and preparative properties. This study used the JEOL IT 500 field emission scanning electron microscope (SEM) to characterize the surface morphology..

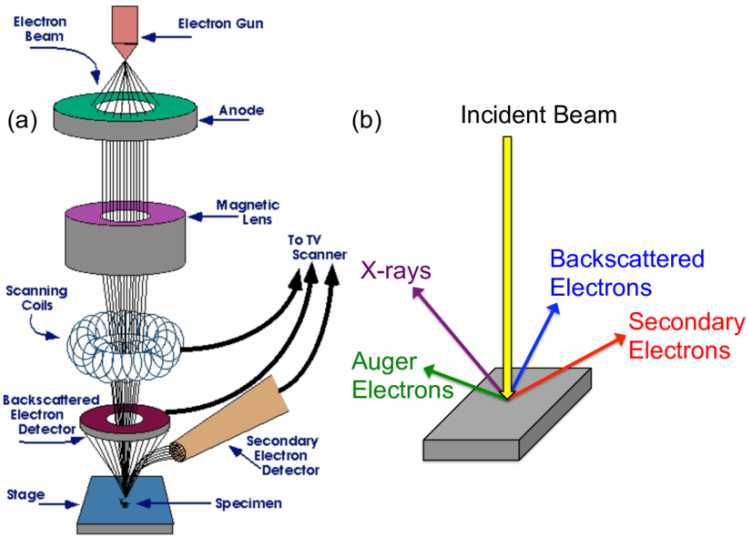

Figure 2.7 Schematic diagram of scanning electron microscope[55]

As can be seen in Figure 2.7, the electron gun releases a powerful electron beam that is aimed straight down at the sample which is positioned vertically. The anode assists in beam acceleration, and the magnetic lenses maintain their position to give the rushing electrons the correct vertical direction. The electrons collide with the surface electron as soon as they strike the sample, scattering the electrons until they reach the detector. The detector then transforms the signal into an electric signal and releases the morphological image.

2.2.4 Energy Dispersive X-ray Spectroscopy (EDX)

Energy-dispersive X-ray spectroscopy (EDX) is a non-destructive analytical technique used to determine the elemental composition of a sample. It is often employed in conjunction with scanning electron microscopy (SEM) or transmission electron microscopy (TEM) to provide detailed information about the spatial distribution of elements within a material. EDX works based on the principle of X-ray fluorescence. When a high-energy electron beam interacts with the atoms in a sample, it causes the emission of characteristic X-rays corresponding to the atomic structure of the elements present. The energies of these X-rays are characteristic of the elements from which they originate. EDX analysis is typically performed using an energy-dispersive X-ray spectrometer attached to an electron microscope. The spectrometer consists of an X-ray detector, a solid-state detector or scintillator, and associated electronics for signal processing and analysis.

2.3 Electrochemical Characterization

The examination of the chemical characteristics acquired against an applied current or bias is known as electrochemical characterization. Conducting electrochemical studies is necessary to understand the qualities such as redox behavior and electron/mass transport phenomena, which will help to clarify the sample attributes discussion. This technique makes use of an electrolytic solution, a three-electrode cell setup, and Metrohm Autolab Potentiostats for experimentation.

2.3.1 Cyclic Voltammetry (CV)

Cyclic Voltammetry (CV) is a widely used electrochemical technique for studying the redox properties and electrochemical behavior of materials[56]. It operates on the principle of applying a potential sweep to an electrode immersed in an electrolyte solution. As the potential is swept linearly with time, redox reactions occur at the electrode surface, resulting in changes in the current flowing through the cell. The resulting voltammogram, a plot of current versus applied potential, provides insights into the kinetics, reversibility, and mechanisms of the electrochemical reactions. Two conventions are used to report the CV data: the US convention and the IUPAC convention. Visually data reported in the two conventions will appear to be rotated by 180^0(Figure 2.8).

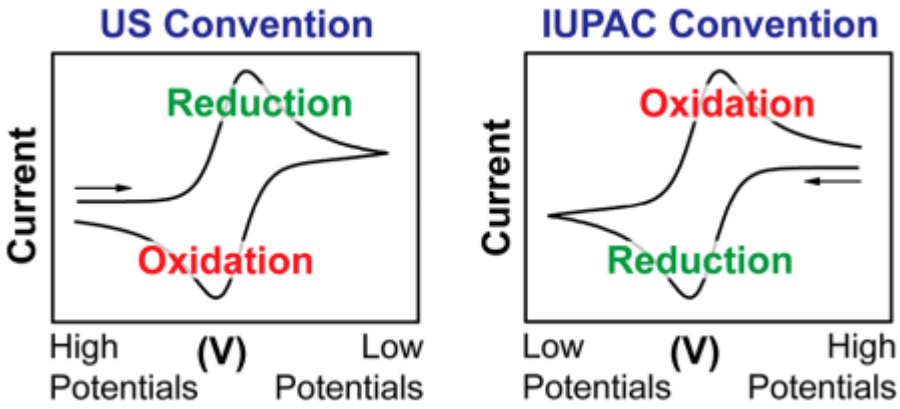

Figure 2.8 Typical Cyclic voltammetry curves[56]

2.3.2 Galvanostatic Charge Discharge (GCD)

This method involves applying a steady current and letting the sample charge (or discharge) over time. It is frequently employed to describe

materials that exhibit capacitive or pseudo-captivate behavior. Greater charge storage capacity and, thus, improved capacitive characteristics are associated with longer discharge times in the material.

2.3.3 Electrochemical Impedance Spectroscopy (EIS)

This instrument records a sample's impedance through the application of AC potentials. EIS is used to get data on things like double-layer capacitance and electron transfer resistance.
It is typically stated in terms of Nyquist and Bode graphs.

- **Bode plot:** This graph, which shows the phase of the sample, is created by graphing the log of impedance on the Y-axis against the log of frequency on the X-axis.
- **Nyquist plot:** Plotting the imaginary component of the impedance (Z'') against the real part (Z') yields the Nyquist plot, which can be used to fit an electrical circuit or be used to directly retrieve a number of circuit parameters.

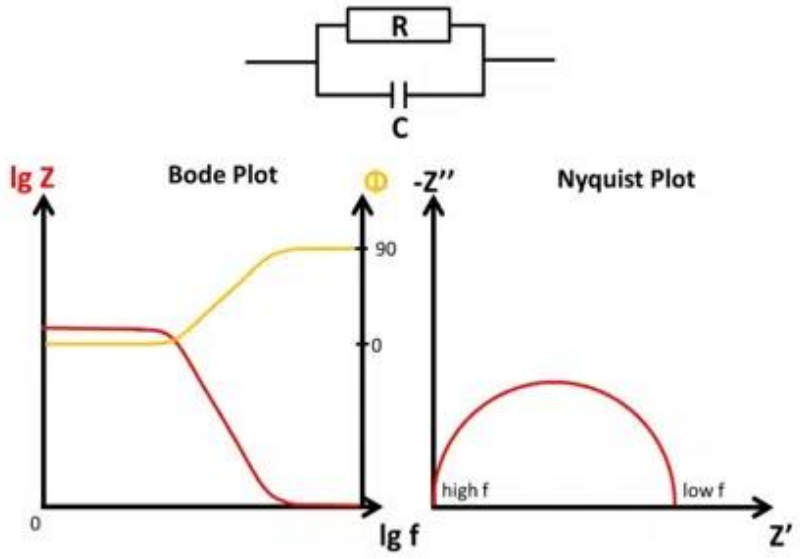

Figure 2.9 : Typical pattern of Bode and Nyquist plots[57]

Chapter 3

RESULTS AND DISCUSSIONS

Section A. Structural and Morphological Analysis

3.1 Characterization of CED Cobalt Sulfide Film

3.1.1 X-ray Diffraction (XRD) Analysis

In order to examine the structure of the continuous electrodeposited (CED) cobalt sulfide films on the FTO substrate, X-ray diffraction analysis was used. Figure 3.1 shows the X-ray diffraction pattern for the continuous electrodeposited Cobalt sulfide. The X-ray diffraction pattern shows peaks at 2θ = 26.4º, 33.6º, 37.7º, 51.4º, 54.5º, 61.5º, 65.4º, 78.2º values. All these peaks are characteristic peaks corresponding to the standard of SnO2 (PDF 46–1088) and deriving from the FTO substrate. No additional peak corresponding to crystalline cobalt sulfide has been observed. The absence of characteristic diffraction peaks for crystalline cobalt sulfide suggests the existence of the amorphous nature of the deposited film. This amorphous behavior has also been validated by the available literature[58–60].

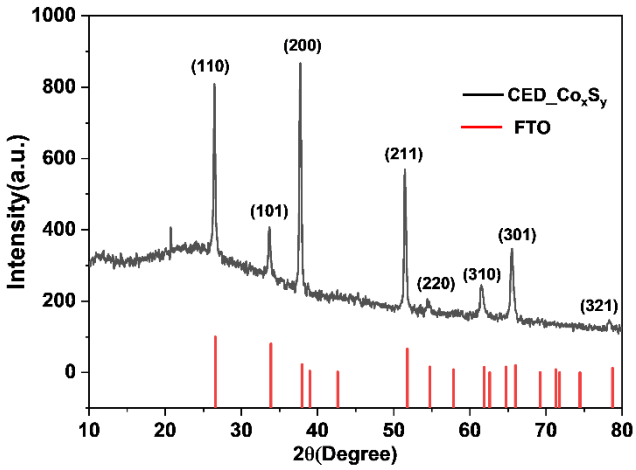

Figure 3.1 XRD pattern of CED cobalt sulfide film

3.1.2 Scanning Electron Microscopy (SEM)

Morphological information of continuous electrodeposited (CED) cobalt sulfide film is obtained by using scanning electron microscopy. SEM images shown in Figure 3.2, revealed non-uniform surface coverage and particle agglomeration in the cobalt sulfide film deposited via continuous electrodeposition. The film exhibited irregularities and uneven growth onto the substrate. It also confirms the amorphous nature of the deposited film as suggested by the X-ray diffraction in section 3.1.1.

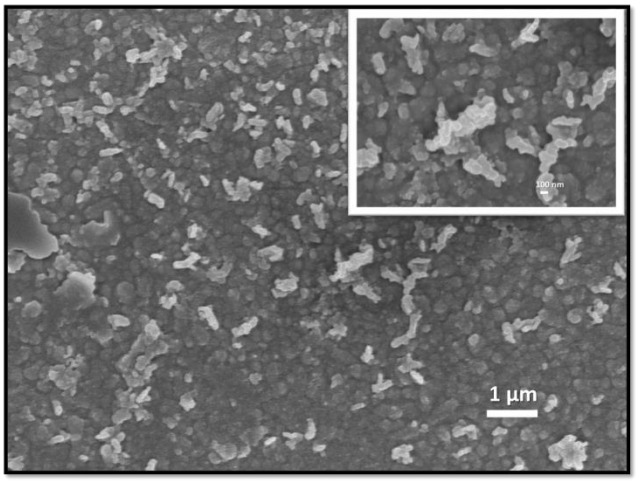

Figure 3.2 SEM image of CED cobalt sulfide film at scale of 1 µm and 100 nm (inset).

3.1.3 EDX Spectrum

Energy-dispersive X-ray spectroscopy provides information about the elements included in the sample. Here EDX spectrum (Figure 3.3) shows the peaks corresponding to Co (Cobalt), and S (Sulfur) elements which confirm the presence of these elements in the continuous deposited film.

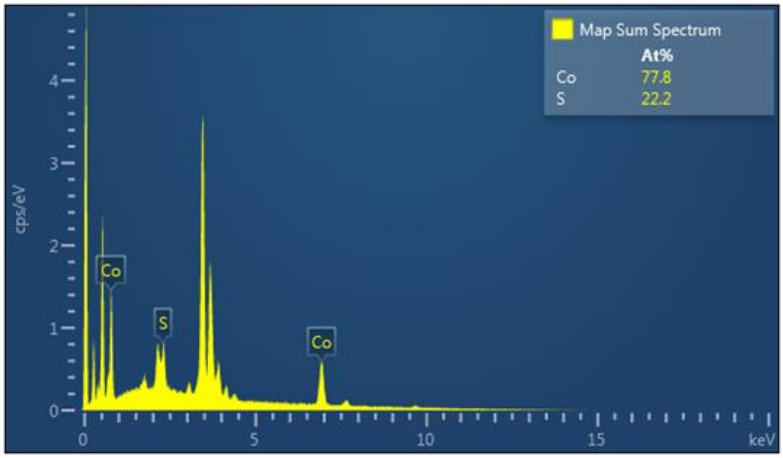

Figure 3.3 EDX spectra of CED Cobalt sulfide film confirms the presence of Co and S in the film

3.1.4 Raman Spectroscopy

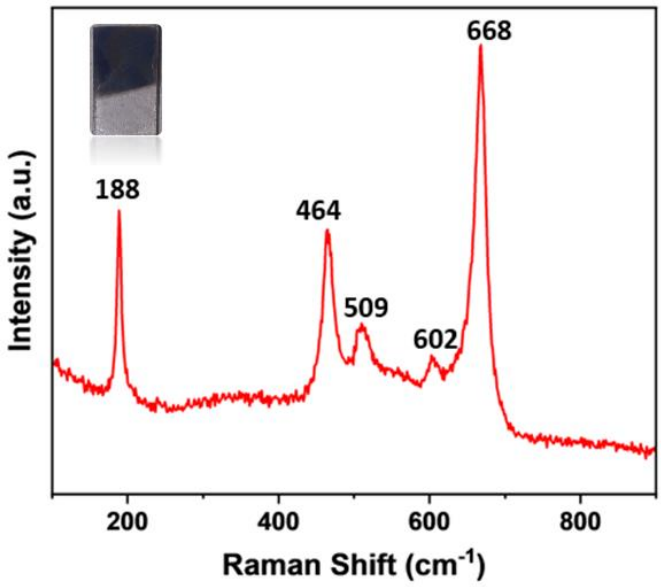

Figure 3.4 Raman Spectra of CED Cobalt Sulfide film, as deposited film (inset).

Figure 3.4 shows five clear and typical bands at 188 cm^{-1}, 464 cm^{-1}, 509 cm^{-1}, 602 $cm^{-1,}$ and 668 cm^{-1} because of the different types of vibration modes (E_g mode, A_{1g} mode, and three modes of vibration). According to the literature the peaks at 464 cm^{-1}, 509 cm^{-1}, 602 cm^{-1} are attributed to vibrational modes of the Co-S bond, and the one at 663 cm^{-1} is due to the involved S-S stretching vibration, representing the formation of cobalt sulfide phase[61].

3.2 Characterization of Pulse Electrodeposited (PED) Cobalt Sulfide Film

3.2.1 X-ray Diffraction (XRD)

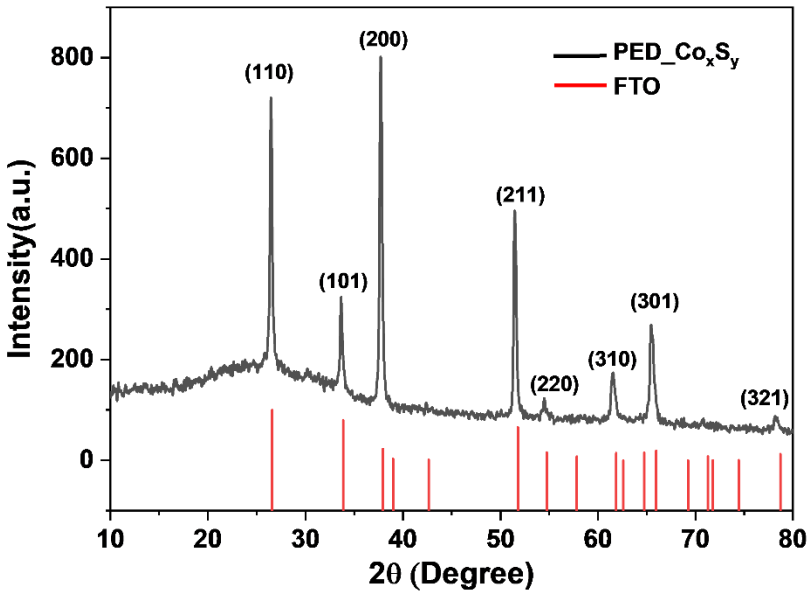

Figure 3.5 XRD pattern of Pulse electrodeposited Cobalt sulfide film

The X-ray diffraction pattern for the pulse electrodeposited film is shown in Figure 3.5. Similar to the CED Cobalt sulfide film, only peaks corresponding to the standard of SnO2 (PDF 46–1088) are observed in the XRD graph which are derived from the FTO substrate. No peaks for the crystalline cobalt sulfide have appeared in the pattern indicating the amorphous nature of the deposited film. This amorphous behavior has also been supported by the available literature[58–60].

3.2.2 Scanning Electron Microscopy (SEM)

Scanning electron microscopy is used to collect morphological information on pulse electrodeposited (PED) cobalt sulfide film. SEM images of the cobalt sulfide film deposited via pulse electrodeposition showed a significant improvement in surface morphology (Figure 3.6). The film displayed enhanced uniformity and smoother surface texture compared to the film deposited via continuous deposition method (Figure 3.2). The difference in morphology between films deposited via continuous and pulse electrodeposition can be fundamentally linked to the differences in growth and nucleation mechanisms inherent to each deposition technique.

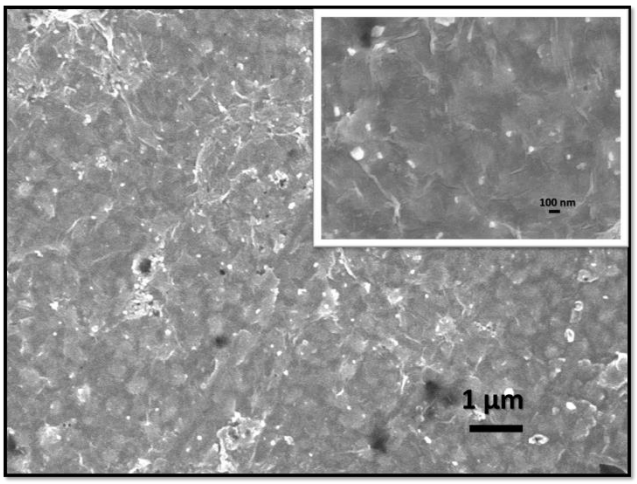

Figure 3.6 SEM image of PED cobalt sulfide film at scale of 1 µm and 100 nm (inset).

3.2.3 EDX Spectra

Energy-dispersive X-ray spectroscopy provides information about the elements included in the sample. Here EDX spectrum (Figure 3.7) shows the peaks corresponding to Co (Cobalt), and S (Sulfur) elements which confirm the presence of these elements in the pulse-deposited film

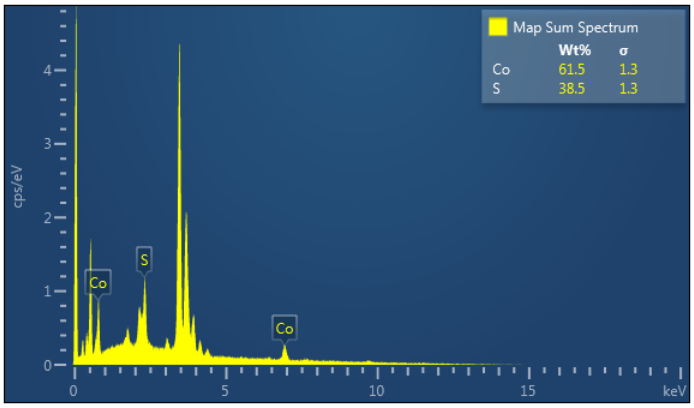

Figure 3.7 EDX spectra of PED Cobalt sulfide film confirm the presence of Co and S in the film.

3.2.4 Raman Spectra

Figure 3.8 shows the Raman spectra of the PED Cobalt sulfide film. Vibrational modes at 676 cm^{-1}, 191 cm^{-1}, and 473 cm^{-1} are corresponding to A_{1g}, $F_{2g,}$ and E_g modes of Co_3S_4 respectively. The primary mode A_{1g} could be attributed to S-S stretching vibration while the F_{2g} and E_g modes could be assigned to the Co-S bonding[62]. A peak at 396 cm^{-1} is a characteristic peak of pure Co_xS_y[63]. A peak at 607 cm^{-1} is due to the typical phonon mode F^1_{2g} while the peak at 283 is assigned to the E_g mode of CoS_2[64,65].

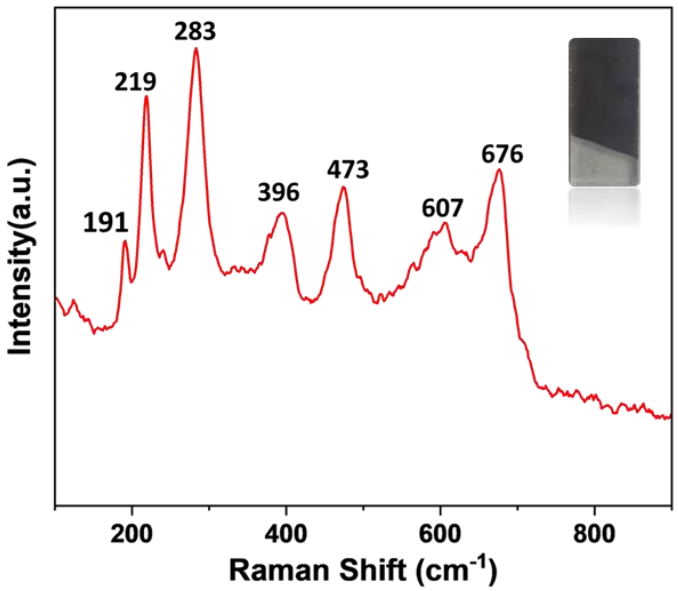

Figure 3.8 Raman Spectra of PED Cobalt Sulfide film, as deposited film (inset).

After confirmation of proper film formation, electrochemical studies were performed on the cobalt sulfide films to investigate redox behavior and supercapacitive nature therein. Various electrochemical characterizations such as cyclic voltammetry, galvanostatic charge-discharge, and electrochemical impedance spectroscopy have been performed.

Section B. Electrochemical Analysis

3.3 Electrochemical Analysis of CED Cobalt Sulfide Film

3.3.1 Cyclic Voltammetry (CV)

Using the setup explained in section 2.3, CV analysis has been for the CED cobalt sulfide in a potential window of -0.3V to 0.7V at various scan rates ranging from 10mV/s to 50mV/s. The electrolyte used is 2M KOH (Potassium Hydroxide) prepared in 20mL DI water. A platinum electrode was used as a Counter/Auxiliary electrode while Ag/AgCl was used as the Reference electrode. Cobalt sulfide deposited onto FTO was used as the working electrode. Figure 3.9 shows the cyclic voltammetry (CV) curves of electrodes fabricated from cobalt sulfide in a 2M KOH solution electrolyte with various scan rates. The shape of CV curves reveals that the capacitance characteristic of the cobalt sulfide is distant from that of the electric double-layer capacitance, which would produce a CV curve with close to an ideal rectangular shape.

The specific Capacitance is given by the formula $\mathbf{C_s} = \frac{\oint \mathbf{IdV}}{\mathbf{2\nu m\Delta V}}$, Where $\oint$ IdV is the area under the

CV curve, m is the mass of the active material, ΔV is the potential window of the CV curve. The average mass loaded on the FTO substrate of cobalt sulfide was 0.001g.

.

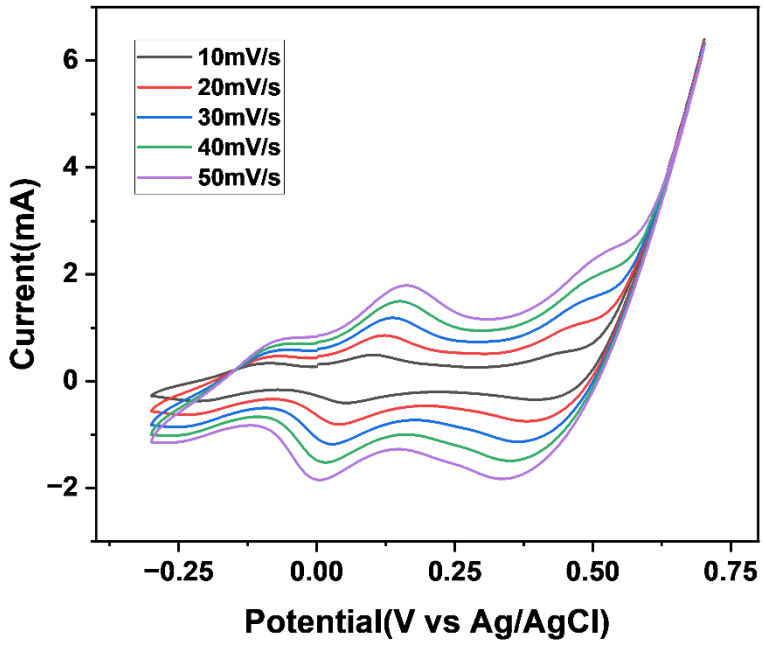

Figure 3.9 Cyclic voltammograms of CED cobalt sulfide at different scan rates (10-50 mV/s)

Sr. No.	Scan rate (mV/s)	Mass deposited (g)	Mathematical Area (mA-V)	Specific capacitance (F/g)
1	10	0.001	0.47411	23.70
2	20	0.001	0.87474	21.87
3	30	0.001	1.25569	20.93
4	40	0.001	1.62173	20.27
5	50	0.001	1.98311	19.83

Table 3.1 Comparison of specific capacitance vs Scan rate for CED cobalt sulfide

It shows that the obtained specific capacitance is decreased with a further increase in scan rate (Table 3.1). This is due to the fact that at a higher scan rate, the electrolyte ions access only the outer region of electrode material which results in a decrease in specific capacitance. However, at a lower scan rate, the electrolyte ions are able to access the inner regions of the active material and thus provide higher specific capacitance. The maximum specific capacitance of the cobalt sulfide calculated from the CV curves is 23.70 F/g at a scan rate of 10 mV/s. The plot of specific capacitance vs scan rate is shown in Figure 3.10 to visualize more clearly the variation of specific capacitance.

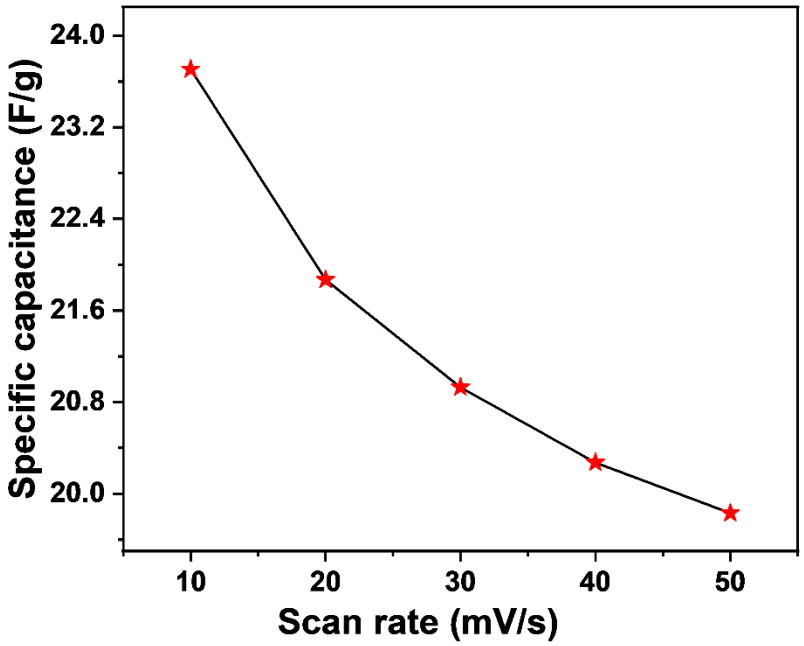

Figure 3.10 Variation of specific capacitance with respect to scan rate for CED cobalt sulfide.

Dunn power law relation[66] is used in order to have a deeper understanding of the electrode material's charge storage mechanism,

$$i = av^b \quad (1)$$

where i is the current, v is the scan rate, and a and b are adjustable constant. A value of b = 0.5 indicates the dominance of the diffusion-controlled process, whereas b = 1 indicates the dominance of surface capacitance. To further quantify this, the above-mentioned equation (1) can be rearranged to get the following equation (2)

$$log(i) = log(a) + b\ log(v) \quad (2)$$

using the above equation (2), the value of b is calculated using the slope value of the plot of *log(i) vs log(v)* (Figure 3.11), which is found to be b = 1.21 obtained by fitting the graph for CED cobalt sulfide at 0V. It indicates the dominance of surface capacitance on the current response of CED cobalt sulfide.

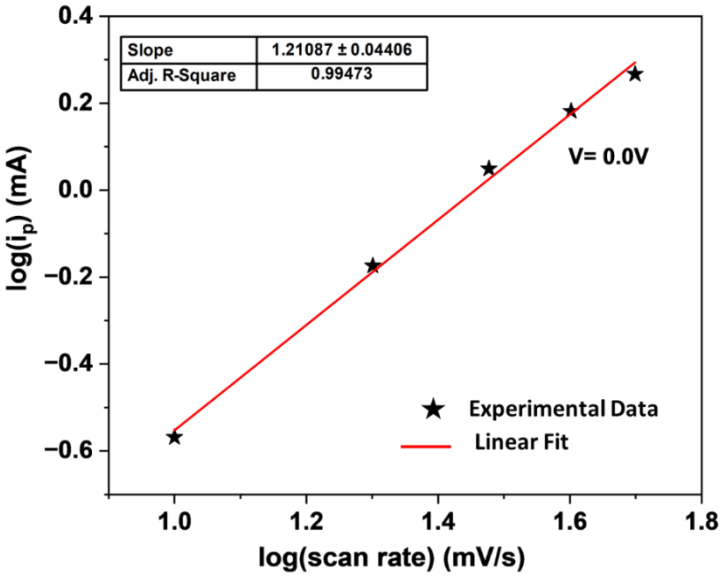

Figure 3.11 Variation of log(current) vs log(scan rate) for CED cobalt sulfide at V=0 V.

Morover, the **Dunn method**[66] is used to determine the total capacitive nature contribution from diffusion-controlled capacitance and surface capacitance, as shown below

$$i = k_1 v + k_2 v^{1/2} \quad (3)$$

For analytical purposes, we rearrange this slightly to

$$\frac{i}{v^{1/2}} = k_1 v^{1/2} + k_2 \quad (4)$$

where k_1 v and k_2 $v^{1/2}$ represent the current response for surface capacitance and diffusion-controlled contributions, respectively, and the values of k_1 and k_2 are calculated from the slope and intercept values, respectively, from the graph of $i/ v^{1/2}$ vs $v^{1/2}$ plotted at 0 V (Figure 3.12). The calculated values (using equations (3) and (4)) of k_1 and k_2 from the fitting of the graph come out to be 0.046 and -0.056, respectively. On putting the values of k_1 and k_2 in the Dunn equation, it is found that 72% of the current at 10 mV/s is contributed due to surface capacitance and increases up to 85% at a scan rate of 50 mV/s (Figure 3.13).

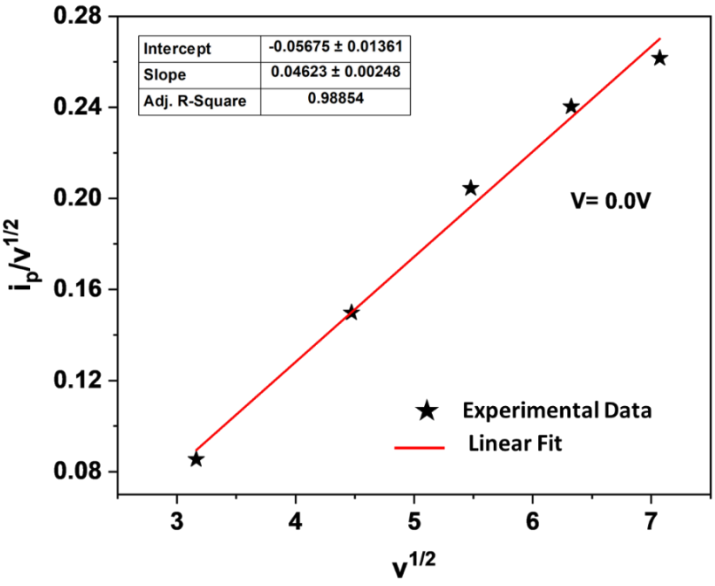

Figure 3.12 Variation of $i/ v^{1/2}$ with respect to $v^{1/2}$ for CED cobalt sulfide

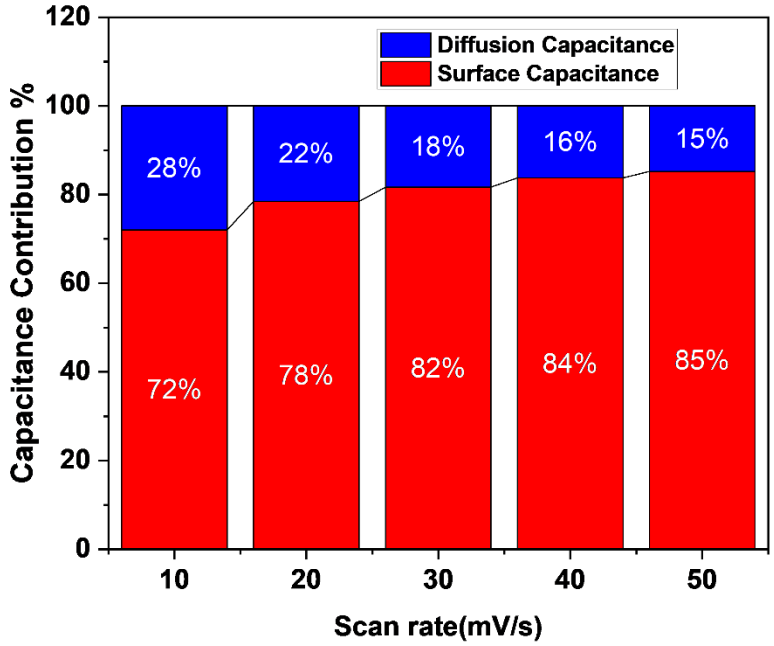

Figure 3.13 Diffusion capacitance and surface capacitance contributions to the overall capacitance at different scan rates for CED cobalt sulfide

3.3.2 Galvanostatic Charge Discharge (GCD)

It's critical to comprehend a supercapacitor's charging and discharging characteristics in order to evaluate its performance. Supercapacitors must be charged quickly and emptied slowly in order to have a high energy density and power density. Figure 3.14 shows the GCD curves for CED cobalt sulfide at different constant currents (0.1-1 mA) within a wide potential window of +0.45 to −0.1 V. The value of specific capacitance is also calculated from the GCD curves using the following formula,

$$C_s = \frac{I\,\Delta t_d}{m\,\Delta V},$$

Where C_s is the specific capacitance, Δt_d is discharging time, m is the deposited mass, I is the current and ΔV is the discharging potential window. The value of specific capacitance calculated using CV curve and GCD curve ais same to some extent.

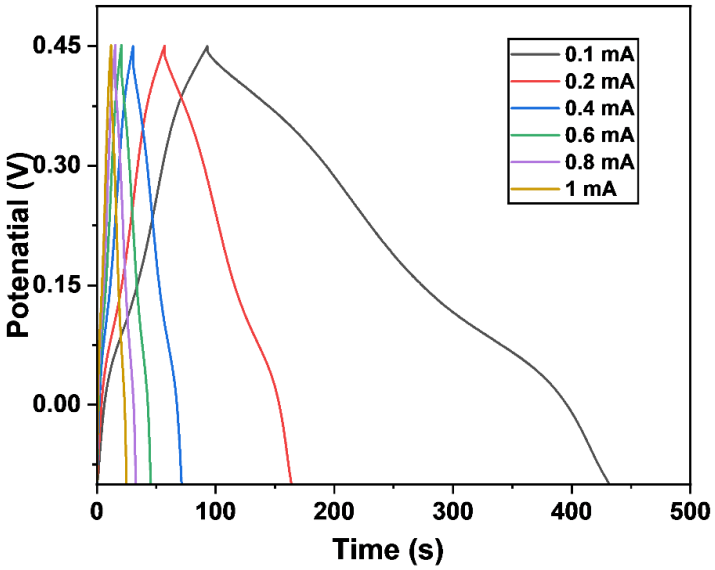

Figure 3.14 GCD curves for CED cobalt sulfide at different constant currents (0.1-1 mA)

In the below table 3.2 T_1 and T_2 represent total time and charging time respectively. With increasing values of currents specific capacitance decreases as since it depends on the product of current and discharging time. These factors govern the value of specific capacitance at a particular value of current. Figure 3.15 is giving the current density-dependent variation of specific capacitance.

Sr. No.	**I (mA)**	**T_1 (s)**	**T_2 (s)**	**T_1-T_2 = Δt_d (s)**	**Mass deposited(m) (g)**	**ΔV (Volt)**	**Specific capacitance C_s (F/g)**
1	0.1	432	93	339	0.001	0.54	62.3
2	0.2	164	57	107	0.001	0.54	39.6
3	0.4	71.5	30.5	41	0.001	0.53	31.1
4	0.6	45.5	21	24.5	0.001	0.52	28.7
5	0.8	33	15.5	17.5	0.001	0.51	27.3
6	1	25	12	13	0.001	0.50	26.1

Table 3.2 Specific capacitance using charging and discharging cycle of the CED cobalt sulfide

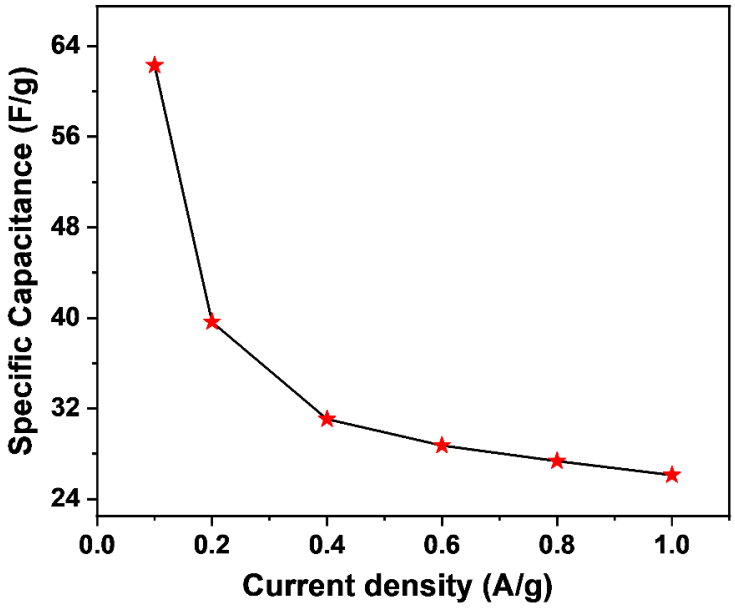

Figure 3.15 Variation of specific capacitance with current density for CED cobalt sulfide.

3.3.3 Electrochemical Impedance Spectroscopy (EIS)

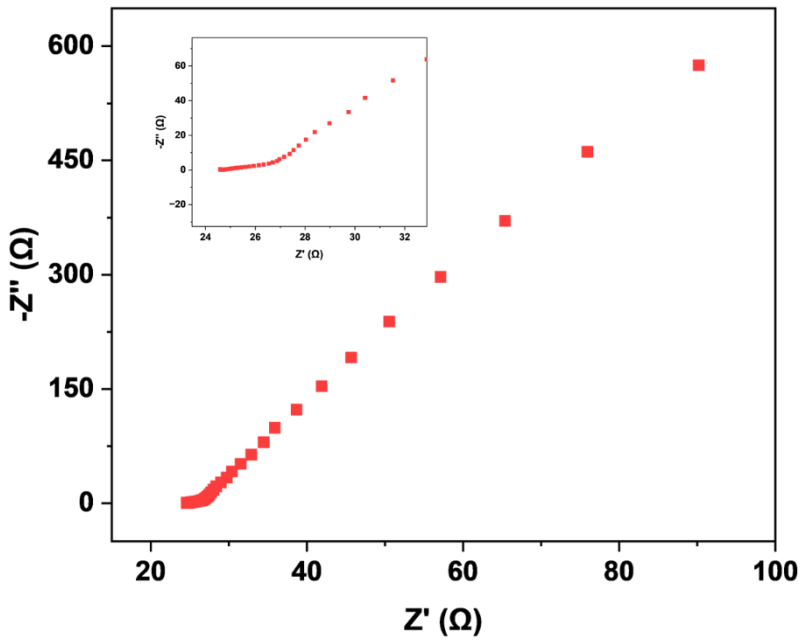

Figure 3.16 Nyquist plot for CED cobalt sulfide showing the variation of imaginary impedance with real impedance value

With an alternating current (AC) amplitude of 20 mV and a frequency range of 10 kHz to 10 mHz, electrochemical impedance analysis was performed in order to better comprehend the ion diffusion mechanism in the CED cobalt sulfide electrode. The ionic resistance of electrolytes, intrinsic resistance of electrodes, and ion diffusion work together to produce the solution resistance (R_s). On the other hand, contact resistance at different interfaces and the electronic resistance of the electrode material contribute to the charge transfer resistance (R_{ct}).

3.4 Electrochemical Analysis of PED Cobalt Sulfide Film

3.4.1 Cyclic Voltammetry (CV)

CV analysis has been for the PED cobalt sulfide in a potential window of -0.2V to 0.7V at various scan rates ranging from 10mV/s to 50mV/s. The electrolyte used is 2M KOH (Potassium Hydroxide) prepared in 20mL DI water. A platinum electrode was used as a Counter/Auxiliary electrode while Ag/AgCl was used as the Reference electrode. Cobalt sulfide deposited onto FTO was used as the working electrode. Figure 3.17 shows the cyclic voltammetry (CV) curves of electrodes fabricated from cobalt sulfide in a 2M KOH solution electrolyte with various scan rates.

The specific Capacitance is given by the formula $\mathbf{C_s} = \frac{\oint \mathbf{IdV}}{\mathbf{2\nu m\Delta V}}$, Where $\oint$ IdV is the area under the CV curve, m is the mass of the active material, ΔV is the potential window of the CV curve. The average mass loaded on the FTO substrate of cobalt sulfide was 0.001g. One redox peak is observed. Also PED cobalt sulfide film was showing color change during CV, which has not been observed in CED cobalt sulfide film. PED cobalt sulfide film changes its color from light black (at 0.7 V) to yellowish transparent (-0.2V).

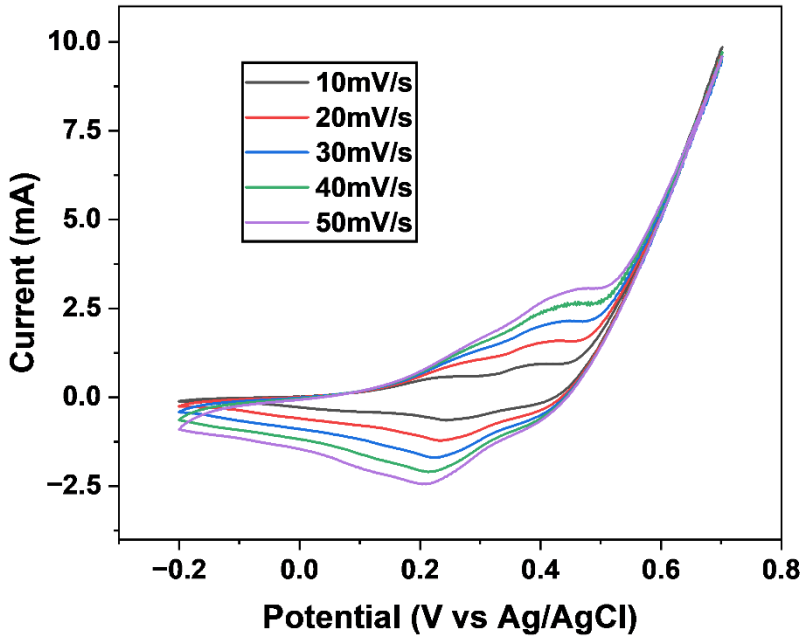

Figure 3.17 Cyclic voltammograms of PED cobalt sulfide at different scan rates (10-50 mV/s).

Sr. No.	Scan rate (mV/s)	Mass deposited (g)	Mathematical Area (mA-V)	Specific capacitance (F/g)
1	10	0.001	0.45435	25.24
2	20	0.001	0.81554	22.65
3	30	0.001	1.13422	21.00
4	40	0.001	1.40594	19.52
5	50	0.001	1.63777	18.19

Table 3.3 Comparison of specific capacitance vs Scan rate for PED cobalt sulfide.

It demonstrates that an additional increase in scan rate results in a drop in the obtained specific capacitance (Table 3.3). The maximum value of specific capacitance of the cobalt sulfide calculated from the CV curves is 25.24 F/g at a scan rate of 10 mV/s. Figure 3.18 displays the plot of specific capacitance versus scan rate to further illustrate how specific capacitance varies.

.

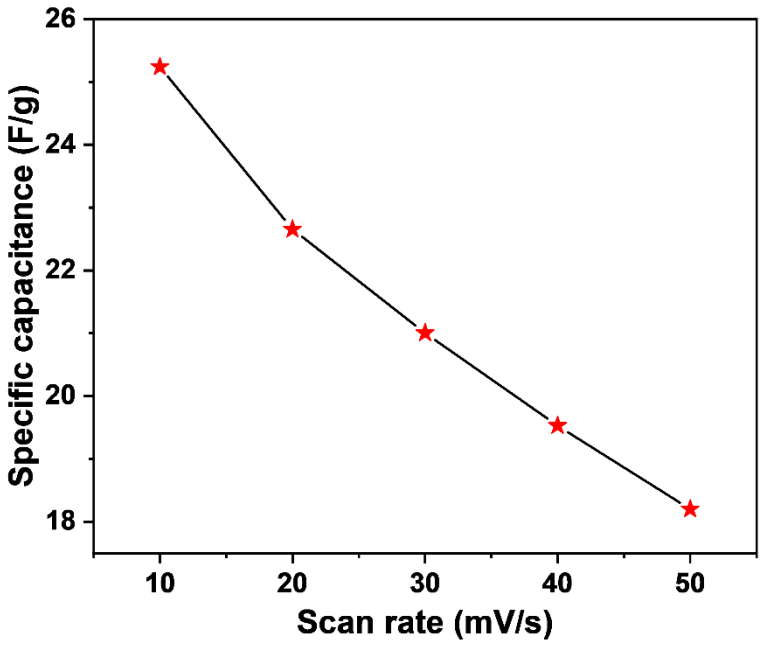

Figure 3.18 Variation of specific capacitance with respect to scan rate for PED cobalt sulfide.

The charge storage mechanism has been studied using the Dunn method (see equation (1) in section 3.3.1).

$$log(i) = log(a) + b\ log(v)$$

using the above equation, the value of *b* is calculated using the slope value of the plot of *log(i) vs log(v)* (Figure 3.19), which is found to be *b* = 0.93 obtained by fitting the graph for PED cobalt sulfide at 0.2 V. It indicates

the dominance of surface capacitance on the current response of PED cobalt sulfide.

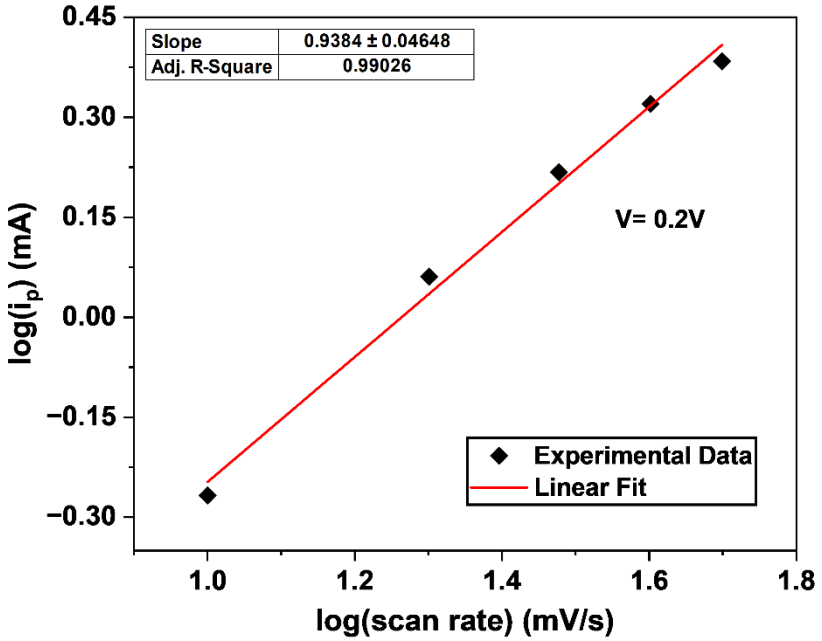

Figure 3.19 Variation of log(current) vs log(scan rate) for PED cobalt sulfide at V=0.2 V.

Additionally, using the Dunn method, the total capacitive nature contribution from diffusion-controlled capacitance and surface capacitance is determined.

$$i = k_1 v + k_2 v^{1/2}$$

where $k_1 \nu$ and $k_2 \nu^{1/2}$ denotes the current response for surface capacitance and diffusion-controlled contributions, respectively, and the values of k_1 and k_2 are derived from the slope and intercept values, respectively, from the graph of $i/\nu^{1/2}$ vs $\nu^{1/2}$ plotted at 0.2 V (Figure 3.20). The calculated values (using equations (3) and (4), see section 3.3.1) of k_1 and k_2 from the fitting of the graph come out to be 0.044 and 0.046, respectively. On

putting the values of k_1 and k_2 in the Dunn equation, it is found that 75% of the current at 10 mV/s is contributed due to surface capacitance and increases up to 87% at a scan rate of 50 mV/s (Figure 3.21).

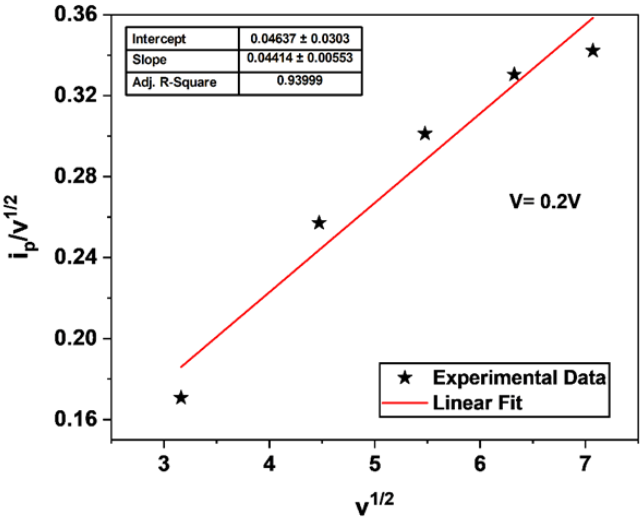

Figure 3.20 Variation of i/ $v^{1/2}$ with respect to $v^{1/2}$ for PED cobalt sulfide.

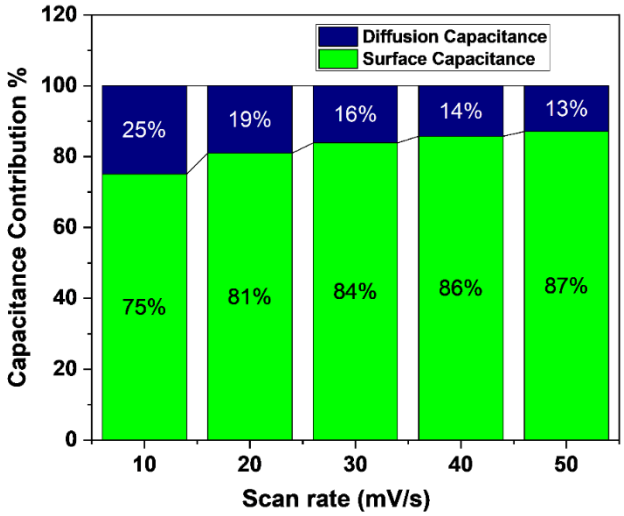

Figure 3.21 Diffusion and surface capacitance contributions to the overall capacitance at different scan rates for PED cobalt sulfide.

3.4.2 Galvanostatic Charge Discharge (GCD)

For supercapacitors to have high energy density and power density, fast charging and slow discharging are essential. Figure 3.22 shows the GCD curves for PED cobalt sulfide at different constant currents (0.1-1 mA) within a wide potential window of +0.42V to −0.1 V. The value of specific capacitance is also calculated from the GCD curves using the following formula,

$$C_s = \frac{I\,\Delta t_d}{m\,\Delta V},$$

Where C_s is the specific capacitance, Δt_d is discharging time, m is the deposited mass, I is the current and ΔV is the discharging potential window.

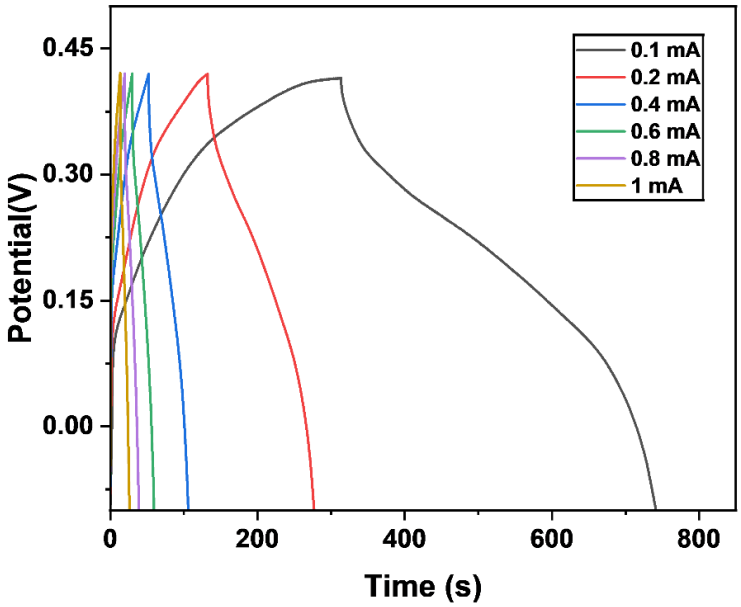

Figure 3.22 GCD curves for PED cobalt sulfide at different constant currents (0.1-1 mA)

In the table 3.4 T_1 and T_2 represent total time and charging time respectively. With increasing values of currents specific capacitance decreases as since it depends on the product of current and discharging time. These factors govern the value of specific capacitance at a particular value of current. Figure 3.23 gives the current density-dependent variation of specific capacitance.

Sr. No.	**I (mA)**	**T_1 (s)**	**T_2 (s)**	**T_1-T_2 = Δt_d (s)**	**Mass deposited(m) (g)**	**ΔV (Volt)**	**Specific capacitance C_s (F/g)**
1	0.1	741	314	427	0.001	0.51	84.2
2	0.2	277	132	145	0.001	0.51	56.9
3	0.4	106	52	54	0.001	0.50	43.3
4	0.6	59.5	30	29.5	0.001	0.48	36.9
5	0.8	39	20	19	0.001	0.47	32.7
6	1	26	13	13	0.001	0.45	27.7

Table 3.4 Specific capacitance using the charging and discharging cycle of the PED cobalt sulfide

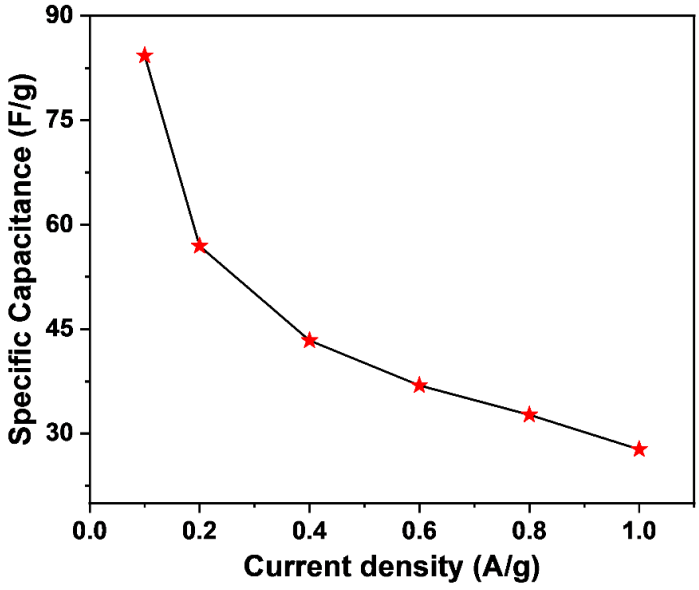

Figure 3.23 Variation of specific capacitance with current density for PED cobalt sulfide.

3.4.3 Electrochemical Impedance Spectroscopy (EIS)

An alternating current (AC) amplitude of 20 mV was used for the electrochemical impedance measurement, which was conducted in the 10 kHz to 10 mHz frequency range. Diffusion of ions, intrinsic resistance of electrodes, and ionic resistance of electrolytes work together to produce the solution resistance (R_s). On the other hand, the electrode material's electronic resistance and the contact resistance at different interfaces contribute to the charge transfer resistance (R_{ct}).

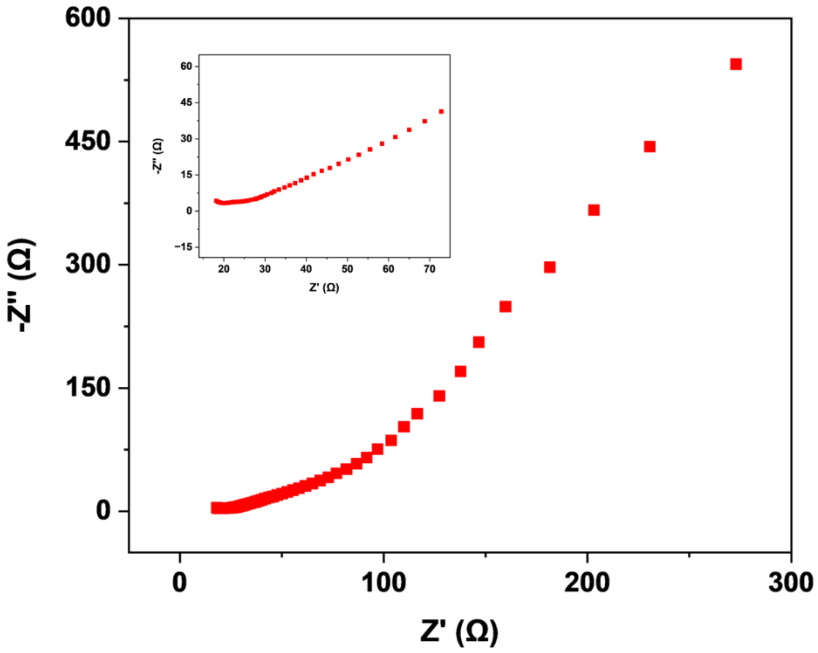

Figure 3.24 Nyquist plot for PED cobalt sulfide showing the variation of imaginary impedance with real impedance value.

3.5 Comparative Electrochemical Study of CED and PED Cobalt Sulfide

In the previous sections 3.3 and 3.4 we have discussed about the electrochemical characterization of continuous electrodeposited and pulse electrodeposited cobalt sulfide film. The maximum specific capacitance of CED cobalt sulfide film, as determined by GCD, is 62.3 F/g at a current of 0.1mA, while as determined by CV, it is 23.7 F/g at a scan rate of 10mV/s. Whereas the maximum specific capacitance of PED cobalt sulfide film, as calculated from GCD, is 84.2 F/g at the current of 0.1mA, while as calculated from CV, it is 25.2 F/g at the scan rate of 10mV/s. We can say that at a low scan rate and low current, the PED cobalt sulfide film shows greater specific capacitance values as compared to the CED cobalt sulfide film. Thus, we have taken PED cobalt sulfide and its suitability for making a supercapacitor is tested by fabricating a device using PED Cobalt sulfide deposited FTO and activated carbon deposited FTO as positive and negative electrode material respectively, and Whatman paper as a separator by following a recipe mentioned in the experimental section 2.1.2. Figure 3.25 shows a comparative CV curve for CED and PED at scan rate of 30mV/s and GD curve at 0.2mA current.

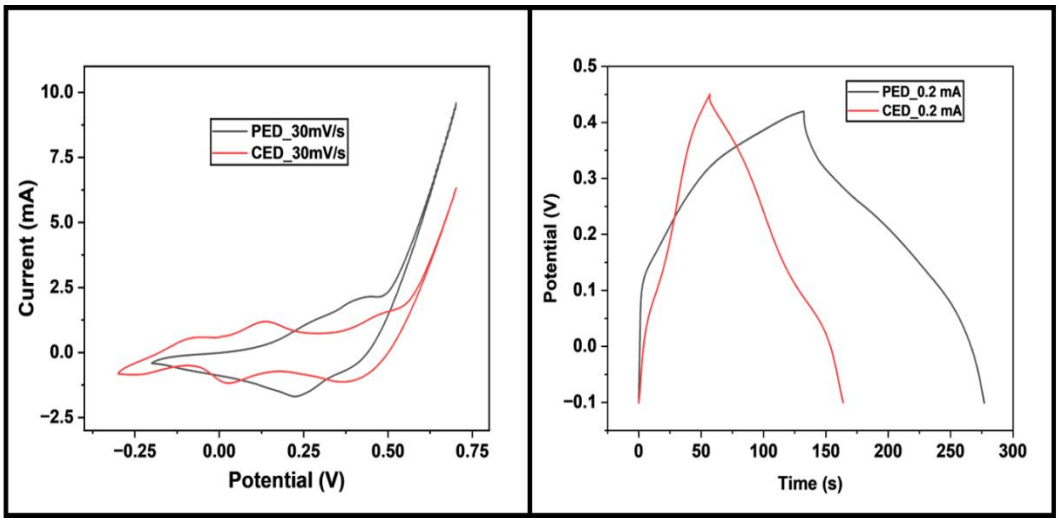

(a) (b)

Figure 3.25 Comparison graphs of CED and PED cobalt sulfide (a) CV at a scan rate of 30mV/s (b) GCD at current 0.2 mA

3.6 Electrochemical analysis of 'PED-Cobalt Sulfide//Activated-Carbon Supercapacitor' Device

All the electrochemical performance of PED-Cobalt sulfide//Activated-carbon device is done in two-electrode cell configurations. The electrochemical performance of the PED-Cobalt sulfide//Activated-carbon device was measured using CV and EIS. The CV curves of the device (in a potential window of 0 to +1.7 V) recorded at various scan rates of 10-50 mV/s (Figure 3.26). It shows that the peak current value for a fabricated device is greater than the peak current value of the PED cobalt sulfide electrode material at a given scan rate, likely due to the large electrode area and the excess mass of deposited material on the device.

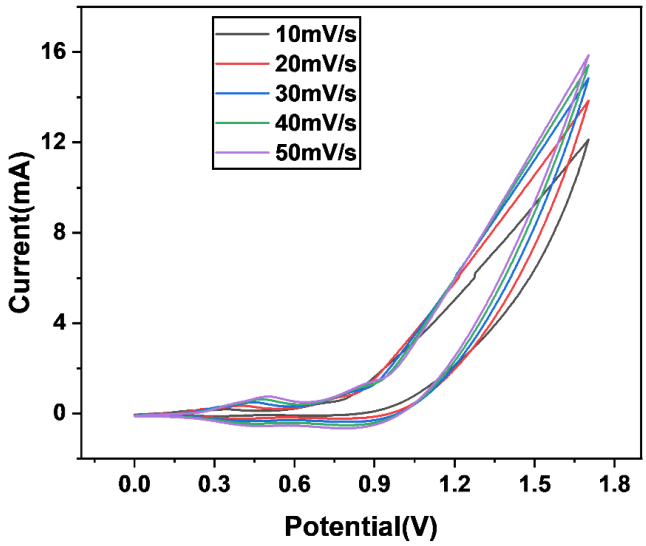

Figure 3.26 CV curves at various scan rates (10, 20, 30, 40, and 50 mV/s)

Specific capacitance has also been calculated from the CV plots using the formula $\mathbf{C_s} = \frac{\oint \mathbf{IdV}}{\mathbf{2vm\Delta V}}$ and variation of specific capacitance with the scan rate has been plotted as shown in Figure 3.27.

The maximum value of specific capacitance observed for PED-Cobalt sulfide//Activated-carbon is 68.5 F/g at a scan rate of 10 mV/s.

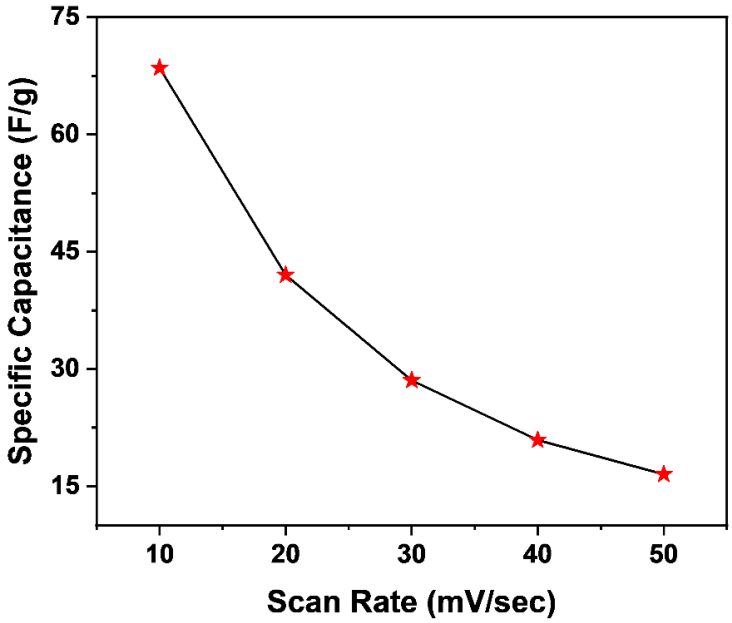

Figure 3.27 Specific capacitance vs scan rate variation for PED cobalt sulfide// activated carbon device

Electrochemical impedance analysis was carried out with the alternating current (AC) amplitude of 20 mV in the frequency range of 100 Hz to 10 mHz (Figure 3.28). The Nyquist plot for the device from EIS data shows a semicircle in the high-frequency range and a diffusion arch in the low-frequency range. The semicircle in the high-frequency region is associated with the solution-electrolyte contact resistance (R_s) and charge transfer resistance (R_{ct}).

On the other hand, the arch at low frequency is related to the ion transport, ion interactions, and redox mechanism occurring at the electrode−electrolyte interface.

Voltage-dependent cyclic voltammetry has also been performed at a scan rate of 50mV/s to show that we can use this device in various potential windows (Figure 3.29). As the potential window widened, the specific capacitance increased because a larger potential window could allow more of the electrode's active material to participate in the electrochemical reactions, thereby storing more charge.

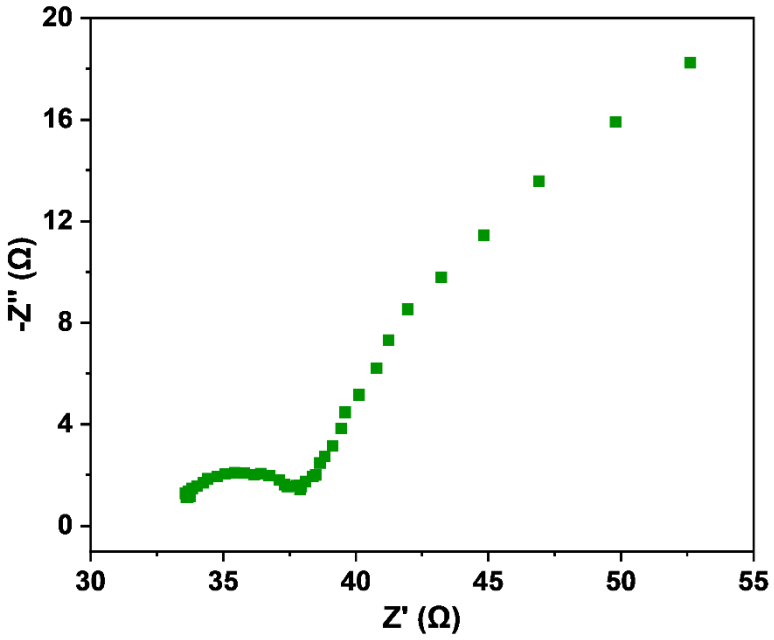

Figure 3.28 Nyquist Plot of PED cobalt sulfide//activated carbon SC device

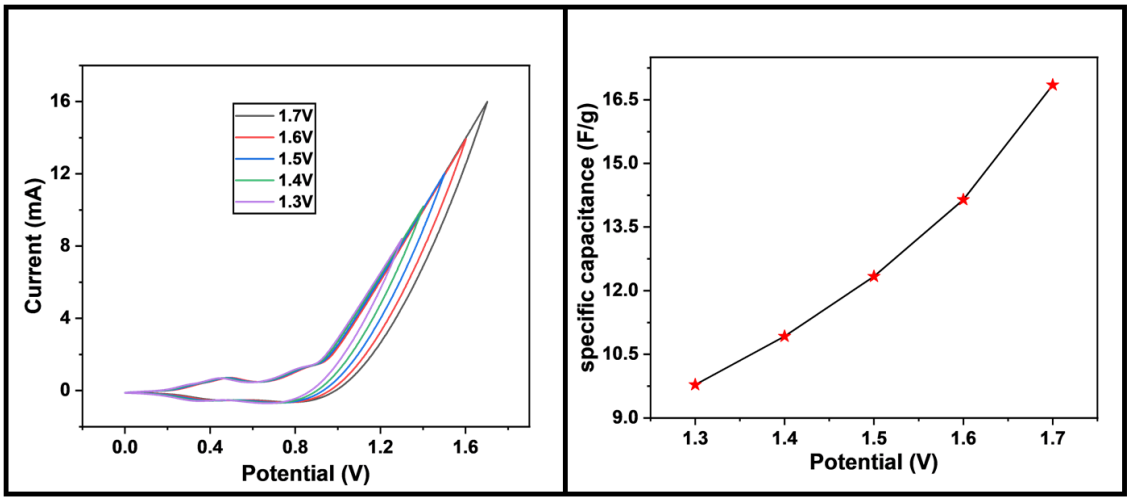

(a) **(b)**

Figure 3.29 (a) Potential dependent CV curve at a scan rate of 50 mV/s (b) Specific capacitance vs Potential window curve for PED cobalt sulfide//activated carbon device

Chapter 4

Conclusion and Future Scope

The new Co_xS_y metal chalcogenide was synthesized using novel pulse electrodeposition and has been compared with simple continuous electrodeposition. The pulse electrodeposited metal chalcogenides show more uniform deposition as compared to CED. Additionally, the CED shows the agglomeration of particles which was absent in PED. The Raman and XRD pattern confirm the deposition which was further confirmed by EDX. Interestingly, the PED-deposited CoS2 shows high electrochemical performance compared to CED which is due to the change in synthesis and hence surface morphology. The electrode shows a high specific capacitance for PED 84 F/g at 0.1 A/g current density whereas CED shows a lower specific capacitance value of 62 F/g at the same current density due to the low solution resistance for PED. Additionally, the surface capacitance contribution for CED is 85% at a 50mV/s scan rate whereas for PED, it is 87% for the same scan rate. The high surface capacitance for PED is due to the smooth surface and small particle size which increases the diffusion of ions from electrolyte to the surface. Then asymmetric supercapacitor device was fabricated whose specific capacitance turned out to be 68.5 F/g and the specific capacitance increased (from 9 F/g to 16 F/g) with the increasing potential window (from 1.3 V to 1.7V) which shows the robust nature of the device. The high specific capacitance value of PED-deposited cobalt sulfide shows its suitability for real-life applications and can be explored further.

Future Scope

Other metal chalcogenides such as nickel sulfide, molybdenum sulfide, tungsten sulfide, etc. as well as tertiary metal sulfides such as nickel-cobalt sulfide, and copper cobalt sulfide can also be explored further. More applications will be searched out in terms of electrochemistry such as electrochromic nature, electrocatalysis behavior, etc.

REFERENCES

(1) Jiang, H.; Zhao, T.; Li, C.; Ma, J. Hierarchical Self-Assembly of Ultrathin Nickel Hydroxide Nanoflakes for High-Performance Supercapacitors. J. Mater. Chem. **2011**, 21 (11), 3818–3823. https://doi.org/10.1039/C0JM03830J.

(2) Bansal, L.; Rani, C.; Ghosh, T.; Kandpal, S.; Chhoker, S.; Tanwar, M.; Kumar, R. Mescoporous Nickel Titanate–Titanium Oxide Complex Material for Enhanced Energy Storage Application. J. Phys. Chem. C **2023**, 127 (19), 8925–8936. https://doi.org/10.1021/acs.jpcc.3c00883.

(3) Ghosh, T.; Kandpal, S.; Rani, C.; Chaudhary, A.; Kumar, R. Recipe for Fabricating Optimized Solid-State Electrochromic Devices and Its Know-How: Challenges and Future. Adv. Opt. Mater. **2023**, n/a (n/a), 2203126. https://doi.org/10.1002/adom.202203126.

(4) Atmaja, T. D.; Amin. Energy Storage System Using Battery and Ultracapacitor on Mobile Charging Station for Electric Vehicle. Energy Procedia **2015**, 68, 429–437. https://doi.org/10.1016/j.egypro.2015.03.274.

(5) Oyedotun, K. Synthesis and Characterization of Carbon-Based Nanostructured Material Electrodes for Designing Novel Hybrid Supercapacitors, 2018. https://doi.org/10.13140/RG.2.2.20007.50084.

(6) Alvarez-Sanchez, C. O.; Lasalde-Ramírez, J. A.; Ortiz-Quiles, E. O.; Massó-Ferret, R.; Nicolau, E. Polymer-MTiO3 (M = Ca, Sr, Ba) Composites as Facile and Scalable Supercapacitor Separators. Energy Sci. Eng. **2019**, 7 (3), 730–740. https://doi.org/10.1002/ese3.299.

(7) Chen, D.; Pang, D.; Zhang, S.; Song, H.; Zhu, W.; Zhu, J. Synergistic Coupling of NiCo2O4 Nanorods onto Porous Co3O4 Nanosheet Surface for Tri-Functional Glucose, Hydrogen-Peroxide Sensors and Supercapacitor. Electrochimica Acta **2020**, 330, 135326. https://doi.org/10.1016/j.electacta.2019.135326.

(8) Bilgen, S. Structure and Environmental Impact of Global Energy Consumption. Renew. Sustain. Energy Rev. **2014**, 38, 890–902. https://doi.org/10.1016/j.rser.2014.07.004.

(9) Alcaraz-Espinoza, J. J.; de Oliveira, H. P. Flexible Supercapacitors Based on a Ternary Composite of Polyaniline/Polypyrrole/Graphite on Gold Coated Sandpaper. Electrochimica Acta **2018**, 274, 200–207. https://doi.org/10.1016/j.electacta.2018.04.063.

(10) Dong, D.; Dhanabalan, S. S.; Elango, P. F. M.; Yang, M.; Walia, S.; Sriram, S.; Bhaskaran, M. Emerging Applications of Metal-Oxide Thin Films for Flexible and Stretchable Electronic Devices. Appl. Phys. Rev. **2023**, 10 (3), 031314. https://doi.org/10.1063/5.0151297.

(11) Erdemir, F.; Güler, O.; Çanakçı, A. Electroless Nickel-Phosphorus Coated Expanded Graphite Paper: Binder-Free, Ultra-Thin, and Low-Cost Electrodes for High-Performance Supercapacitors. J. Energy Storage **2021**, 44, 103364. https://doi.org/10.1016/j.est.2021.103364.

(12) Armand, M.; Tarascon, J.-M. Building Better Batteries. Nature **2008**, 451 (7179), 652–657. https://doi.org/10.1038/451652a.

(13) Jia, X.; Ge, Y.; Shao, L.; Wang, C.; Wallace, G. G. Tunable Conducting Polymers: Toward Sustainable and Versatile Batteries. ACS Sustain. Chem. Eng. **2019**, 7 (17), 14321–14340. https://doi.org/10.1021/acssuschemeng.9b02315.

(14) Bailmare, D. B.; Tripathi, P.; Deshmukh, A. D.; Gupta, B. K. Designing of Two Dimensional Lanthanum Cobalt Hydroxide Engineered High Performance Supercapacitor for Longer Stability under Redox Active Electrolyte. Sci. Rep. **2022**, 12 (1), 3084. https://doi.org/10.1038/s41598-022-06839-8.

(15) Dong, W. J.; Cho, W. S.; Lee, J.-L. Indium Tin Oxide Branched Nanowire and Poly(3-Hexylthiophene) Hybrid Structure for a Photorechargeable Supercapacitor. ACS Appl. Mater. Interfaces **2021**, 13 (19), 22676–22683. https://doi.org/10.1021/acsami.1c05241.

(16) Zhou, J.; Gong, W.; Meng, X.; Zhang, J.; Zhou, X.; Chen, S.; Bielawski, C. W.; Geng, J. A Macrocyclic Amine-Based Electrolyte for Lithium–Sulfur Batteries: Li Ion Encapsulation Regulates Electrode Performance. Appl. Phys. Rev. **2023**, 10 (4), 041407. https://doi.org/10.1063/5.0159107.

(17) Zhou, Y.; Wang, C.-H.; Lu, W.; Dai, L. Recent Advances in Fiber-Shaped Supercapacitors and Lithium-Ion Batteries. Adv. Mater. **2020**, 32 (5), 1902779. https://doi.org/10.1002/adma.201902779.
(18) Jiang, Y.; Liu, J. Definitions of Pseudocapacitive Materials: A Brief Review. ENERGY Environ. Mater. **2019**, 2 (1), 30–37. https://doi.org/10.1002/eem2.12028.
(19) Wang, L. J.; El-Kady, M. F.; Dubin, S.; Hwang, J. Y.; Shao, Y.; Marsh, K.; McVerry, B.; Kowal, M. D.; Mousavi, M. F.; Kaner, R. B. Flash Converted Graphene for Ultra-High Power Supercapacitors. Adv. Energy Mater. **2015**, 5 (18), 1500786. https://doi.org/10.1002/aenm.201500786.
(20) Alam, M.; Karmakar, K.; Pal, M.; Mandal, K. Electrochemical Supercapacitor Based on Double Perovskite Y2NiMnO6 Nanowires. RSC Adv. **2016**, 6 (115), 114722–114726. https://doi.org/10.1039/C6RA23318J.
(21) Pandit, B.; Rondiya, S. R.; Dzade, N. Y.; Shaikh, S. F.; Kumar, N.; Goda, E. S.; Al-Kahtani, A. A.; Mane, R. S.; Mathur, S.; Salunkhe, R. R. High Stability and Long Cycle Life of Rechargeable Sodium-Ion Battery Using Manganese Oxide Cathode: A Combined Density Functional Theory (DFT) and Experimental Study. ACS Appl. Mater. Interfaces **2021**, 13 (9), 11433–11441. https://doi.org/10.1021/acsami.0c21081.
(22) Palaniselvam, T.; Baek, J.-B. Graphene Based 2D-Materials for Supercapacitors. 2D Mater. **2015**, 2 (3), 032002. https://doi.org/10.1088/2053-1583/2/3/032002.
(23) Ali, G. A. M.; Wahba, O. A. G.; Hassan, A. M.; Fouad, O. A.; Feng Chong, K. Calcium-Based Nanosized Mixed Metal Oxides for Supercapacitor Application. Ceram. Int. **2015**, 41 (6), 8230–8234. https://doi.org/10.1016/j.ceramint.2015.02.100.
(24) Kumar, Y.; Pandey, G. P.; Hashmi, S. A. Gel Polymer Electrolyte Based Electrical Double Layer Capacitors: Comparative Study with Multiwalled Carbon Nanotubes and Activated Carbon Electrodes. J. Phys. Chem. C **2012**, 116 (50), 26118–26127. https://doi.org/10.1021/jp305128z.
(25) Bansal, L.; Kandpal, S.; Ghosh, T.; Rani, C.; Sahu, B.; Kumar Rath, D.; Kumar, R. A Supercapacitive All-Inorganic Nano Metal–Oxide Complex: A 180° Super-Bendable Asymmetric Energy Storage Device. J. Mater. Chem. C **2023**, 11 (45), 16000–16009. https://doi.org/10.1039/D3TC02677A.
(26) Goda, E. S.; ur Rehman, A.; Pandit, B.; Al-Shahat Eissa, A.; Eun Hong, S.; Ro Yoon, K. Al-Doped Co9S8 Encapsulated by Nitrogen-Doped Graphene for Solid-State Asymmetric Supercapacitors. Chem. Eng. J. **2022**, 428, 132470. https://doi.org/10.1016/j.cej.2021.132470.
(27) Guo, Y.; Li, W.; Yu, H.; Perepichka, D. F.; Meng, H. Flexible Asymmetric Supercapacitors via Spray Coating of a New Electrochromic Donor–Acceptor Polymer. Adv. Energy Mater. **2017**, 7 (2), 1601623. https://doi.org/10.1002/aenm.201601623.
(28) Mescoporous Nickel Titanate–Titanium Oxide Complex Material for Enhanced Energy Storage Application | The Journal of Physical Chemistry C. https://pubs.acs.org/doi/10.1021/acs.jpcc.3c00883 (accessed 2024-05-14).
(29) Pore-Size-Dependent Capacitance and Charging Dynamics of Nanoporous Carbons in Aqueous Electrolytes | The Journal of Physical Chemistry C. https://pubs.acs.org/doi/10.1021/acs.jpcc.2c01121 (accessed 2024-05-14).
(30) Freestanding Three-Dimensional Graphene Macroporous Supercapacitor | ACS Applied Energy Materials. https://pubs.acs.org/doi/10.1021/acsaem.7b00338 (accessed 2024-05-14).
(31) Gel Polymer Electrolyte Based Electrical Double Layer Capacitors: Comparative Study with Multiwalled Carbon Nanotubes and Activated Carbon Electrodes | The Journal of Physical Chemistry C. https://pubs.acs.org/doi/10.1021/jp305128z (accessed 2024-05-14).
(32) Wang, K.; Wang, Y.; Wang, Y.; Hosono, E.; Zhou, H. Mesoporous Carbon Nanofibers for Supercapacitor Application. J. Phys. Chem. C **2009**, 113 (3), 1093–1097. https://doi.org/10.1021/jp807463u.
(33) Du, J.; Yu, Y.; Liu, L.; Lv, H.; Chen, A.; Hou, S. Confined-Space Pyrolysis of Polystyrene/Polyacrylonitrile for Nitrogen-Doped Hollow Mesoporous Carbon Spheres with High

Supercapacitor Performance. ACS Appl. Energy Mater. **2019**, 2 (6), 4402–4410. https://doi.org/10.1021/acsaem.9b00578.
(34) Chen, X.; Mi, H.; Ji, C.; Lei, C.; Fan, Z.; Yu, C.; Sun, L. Hierarchically Porous Carbon Microfibers for Solid-State Supercapacitors. J. Mater. Sci. **2020**, 55 (13), 5510–5521. https://doi.org/10.1007/s10853-020-04376-1.
(35) Ghosh, T.; Bansal, L.; Kandpal, S.; Rani, C.; Rath, D. K.; Sahu, B.; Chhoker, S.; Kumar, R. Multifunctional Electrochromic Hybrid PANI@WO3 Core-Shell for Energy Generation and Storage. J. Energy Storage **2023**, 72, 108640. https://doi.org/10.1016/j.est.2023.108640.
(36) Sahu, B.; Bansal, L.; Rath, D. K.; Kandpal, S.; Ghosh, T.; Ahlawat, N.; Rani, C.; Maximov, M. Y.; Kumar, R. Bendable & Twistable Oxide-Polymer Based Hybrid Electrochromic Device: Flexible and Multi-Wavelength Color Modulation. Mater. Today Electron. **2024**, 7, 100082. https://doi.org/10.1016/j.mtelec.2023.100082.
(37) Hydrothermal synthesis, characterization and electrochemical properties of cobalt sulfide nanoparticles - ScienceDirect. https://www.sciencedirect.com/science/article/pii/S136980011530024X#bbib29 (accessed 2024-05-14).
(38) Iimura, R.; Hasegawa, T.; Yin, S. Electrochromic Behavior Originating from the W6+/W5+ Redox in Aurivillius-Type Tungsten-Based Layered Perovskites. Inorg. Chem. **2022**, 61 (5), 2509–2516. https://doi.org/10.1021/acs.inorgchem.1c03364.
(39) Yang, P.; Mai, W. Flexible Solid-State Electrochemical Supercapacitors. Nano Energy **2014**, 8, 274–290. https://doi.org/10.1016/j.nanoen.2014.05.022.
(40) Electrochemical supercapacitor based on double perovskite Y2NiMnO6 nanowires - RSC Advances (RSC Publishing). https://pubs.rsc.org/en/content/articlelanding/2016/ra/c6ra23318j (accessed 2024-05-14).
(41) Manjakkal, L.; Shakthivel, D.; Dahiya, R. Flexible Printed Reference Electrodes for Electrochemical Applications. Adv. Mater. Technol. **2018**, 3 (12), 1800252. https://doi.org/10.1002/admt.201800252.
(42) Abureden, S. Advanced Nanostructure Materials for Hybrid Supercapacitors. Doctoral Thesis, University of Waterloo, 2017. https://uwspace.uwaterloo.ca/handle/10012/12047 (accessed 2024-05-14).
(43) Surendran, S.; Vijaya Sankar, K.; John Berchmans, L.; Kalai Selvan, R. Polyol Synthesis of α-NiS Particles and Its Physico-Chemical Properties. Mater. Sci. Semicond. Process. **2015**, 33, 16–23. https://doi.org/10.1016/j.mssp.2015.01.012.
(44) Krishnamoorthy, K.; Veerasubramani, G. K.; Radhakrishnan, S.; Kim, S. J. Supercapacitive Properties of Hydrothermally Synthesized Sphere like MoS2 Nanostructures. Mater. Res. Bull. **2014**, 50, 499–502. https://doi.org/10.1016/j.materresbull.2013.11.019.
(45) Fano-Type Wavelength-Dependent Asymmetric Raman Line Shapes from MoS2 Nanoflakes | ACS Physical Chemistry Au. https://pubs.acs.org/doi/full/10.1021/acsphyschemau.2c00021 (accessed 2022-06-06).
(46) Krishnamoorthy, K.; Veerasubramani, G. K.; Radhakrishnan, S.; Kim, S. J. One Pot Hydrothermal Growth of Hierarchical Nanostructured Ni3S2 on Ni Foam for Supercapacitor Application. Chem. Eng. J. **2014**, 251, 116–122. https://doi.org/10.1016/j.cej.2014.04.006.
(47) Huang, G.; Chen, T.; Wang, Z.; Chang, K.; Chen, W. Synthesis and Electrochemical Performances of Cobalt Sulfides/Graphene Nanocomposite as Anode Material of Li-Ion Battery. J. Power Sources **2013**, 235, 122–128. https://doi.org/10.1016/j.jpowsour.2013.01.093.
(48) Kandpal, S.; Ghosh, T.; Rani, C.; Rani, S.; Pathak, D. K.; Tanwar, M.; Bhatia, R.; Sameera, I.; Kumar, R. MoS2 Nano-Flower Incorporation for Improving Organic-Organic Solid State Electrochromic Device Performance. Sol. Energy Mater. Sol. Cells **2022**, 236, 111502. https://doi.org/10.1016/j.solmat.2021.111502.
(49) Kandpal, S.; Ghosh, T.; Rani, C.; Rani, S.; Pathak, D. K.; Tanwar, M.; Bhatia, R.; Sameera, I.; Kumar, R. MoS2 Nano-Flower Incorporation for Improving Organic-Organic Solid State Electrochromic Device Performance. Sol. Energy Mater. Sol. Cells **2022**, 236, 111502. https://doi.org/10.1016/j.solmat.2021.111502.

(50) Complex–Surfactant-Assisted Hydrothermal Synthesis and Properties of Hierarchical Worm-Like Cobalt Sulfide Microtubes Assembled by Hexagonal Nanoplates - Liu - 2010 - Chemistry – A European Journal - Wiley Online Library. https://chemistry-europe.onlinelibrary.wiley.com/doi/10.1002/chem.200903384 (accessed 2024-05-14).
(51) Fundamentals and Principles of Electrode-Position | SpringerLink. https://link.springer.com/chapter/10.1007/978-3-319-44920-3_3 (accessed 2024-05-14).
(52) Electrodeposition of Nanostructured Materials | SpringerLink. https://link.springer.com/book/10.1007/978-3-319-44920-3 (accessed 2024-05-14).
(53) Electrodeposited Cobalt-Sulfide Catalyst for Electrochemical and Photoelectrochemical Hydrogen Generation from Water | Journal of the American Chemical Society. https://pubs.acs.org/doi/epdf/10.1021/ja4094764 (accessed 2024-05-14).
(54) Sci-Hub | | 10.1081/E-ECHP-120037171. https://sci-hub.st/10.1081/E-ECHP-120037171 (accessed 2024-05-15).
(55) Nanocomposite coatings based on quaternary metal-nitrogen and nanocarbon systems. https://www.researchgate.net/publication/281184428_Nanocomposite_coatings_based_on_quaternary_metal-nitrogen_and_nanocarbon_systems?_tp=eyJjb250ZXh0Ijp7ImZpcnN0UGFnZSI6Il9kaXJlY3QiLCJwYWdlIjoiX2RpcmVjdCJ9fQ (accessed 2024-05-15).
(56) A Practical Beginner's Guide to Cyclic Voltammetry | Journal of Chemical Education. https://pubs.acs.org/doi/10.1021/acs.jchemed.7b00361 (accessed 2024-05-15).
(57) Bode and Nyquist Plot - PalmSens. https://www.palmsens.com/knowledgebase-article/bode-and-nyquist-plot/ (accessed 2024-05-15).
(58) Sun, Y.; Liu, C.; Grauer, D. C.; Yano, J.; Long, J. R.; Yang, P.; Chang, C. J. Electrodeposited Cobalt-Sulfide Catalyst for Electrochemical and Photoelectrochemical Hydrogen Generation from Water. J. Am. Chem. Soc. **2013**, 135 (47), 17699–17702. https://doi.org/10.1021/ja4094764.
(59) Tao, F.; Zhao, Y.-Q.; Zhang, G.-Q.; Li, H.-L. Electrochemical Characterization on Cobalt Sulfide for Electrochemical Supercapacitors. Electrochem. Commun. **2007**, 9 (6), 1282–1287. https://doi.org/10.1016/j.elecom.2006.11.022.
(60) Mardosaite, R.; Valatka, E. STRUCTURE AND ELECTROCATALYTIC PROPERTIES OF AMORPHOUS COBALT–SULPHIDE FILMS ON FTO SUBSTRATE.
(61) Ju, S.; Liu, Y.; Chen, H.; Tan, F.; Yuan, A.; Li, X.; Zhu, G. In Situ Surface Chemistry Engineering of Cobalt-Sulfide Nanosheets for Improved Oxygen Evolution Activity. ACS Appl. Energy Mater. **2019**, 2 (6), 4439–4449. https://doi.org/10.1021/acsaem.9b00687.
(62) Cobalt Sulfide Nanosheets as Peroxidase Mimics for Colorimetric Detection of l-Cysteine | ACS Applied Nano Materials. https://pubs.acs.org/doi/10.1021/acsanm.1c02851 (accessed 2024-05-15).
(63) Graphene-based cobalt sulfide composite hydrogel with enhanced electrochemical properties for supercapacitors. https://www.researchgate.net/publication/291386907_Graphene-based_cobalt_sulfide_composite_hydrogel_with_enhanced_electrochemical_properties_for_supercapacitors (accessed 2024-05-15).
(64) Chen, F.; Luo, W.; Mo, Y.; Yu, H.; Cheng, B. In Situ Photodeposition of Amorphous CoSx on the TiO2 towards Hydrogen Evolution. Appl. Surf. Sci. **2018**, 430, 448–456. https://doi.org/10.1016/j.apsusc.2017.06.165.
(65) Electrodeposited Heterostructures of Cobalt Sulfide/Molybdenum Sulfide Trigger both Acidic and Alkaline HER. https://www.researchgate.net/publication/369782698_Electrodeposited_Heterostructures_of_Cobalt_SulfideMolybdenum_Sulfide_Trigger_both_Acidic_and_Alkaline_HER (accessed 2024-05-15).
(66) Pseudocapacitive Contributions to Electrochemical Energy Storage in TiO2 (Anatase) Nanoparticles | The Journal of Physical Chemistry C. https://pubs.acs.org/doi/10.1021/jp074464w (accessed 2024-05-15).